JOURNAL OF GEOPHYSICAL RESEARCH, VOL. 100, NO. C11, PAGES 22,625–22,646, NOVEMBER 15, 1995

Subgrid parameterization of surface heat and momentum fluxes over polar oceans

Timo Vihma

Department of Geophysics, University of Helsinki, Finland

Abstract. The parameterization of heat and momentum fluxes over a heterogeneous surface consisting of sea ice and large areas of open ocean (polynyas) has been studied. Various theories required to calculate grid-averaged fluxes are discussed, and a two-dimensional mesoscale boundary layer model has been applied to simulate the flow and heat exchange processes inside a single grid element of a hypothetical atmospheric general circulation model. The theories are compared with model results. Considering the surface fluxes of sensible and latent heat, a mosaic method, based on the use of estimates for local surface temperature, air temperature, specific humidity, and wind speed over the ice-covered and ice-free parts of the grid square, performed well in the comparison. Parameterizing the net longwave radiation, an estimate for the subgrid distribution of cloudiness was useful. Parameterization of surface momentum flux seemed to be most reasonable on the basis of the surface pressure field and a geostrophic drag coefficient depending on the air-surface temperature difference.

1. Introduction

In polar oceans, especially in wintertime, the ice cover efficiently prevents heat exchange between the relatively warm ocean and the cold atmosphere. There are, however, discontinuities in the ice cover, and these areas of open water may have horizontal dimensions ranging from 1 m to 100 km. The smaller ones, with a typical width of from 1 m to 1 km and length of from 100 m to 100 km, are here called leads and are usually formed by divergent ice drift. Here we use the term polynya for the larger areas of open water, with characteristic horizontal dimensions of from 1 to 100 km or, on rare occasions, even up to 1000 km, as in the case of the Weddell Polynya in 1974-1976. Polynyas are often recurrent or semipermanent in nature. They form most usually along coastlines, if wind carries the ice away from the coast more rapidly than new ice can be formed [*Cavalieri and Martin,* 1985; *Pease,* 1987]. A region of fast ice may remain between the coast and the polynya, as is the case, e.g., for the Laptev Sea Polynya (Figure 1). Polynyas may, however, occur in the middle of the pack-ice field as well (e.g., the Weddell Polynya, the Maud Rise Polynya, and the Cosmonaut Polynya in the Southern Ocean), remaining open due to oceanic heat flux and/or large-scale divergence of surface currents. Reviews of the occurrence and characteristics of leads and polynyas are given by *Zwally et al.* [1985], *Comiso and Gordon* [1987], and *Smith et al.* [1990].

The heat loss from the ocean to the atmosphere through polynyas is efficient and has been the topic of several field experiments in the Arctic [*Andreas et al.,* 1979; *den Hartog et al.,* 1983; *Smith et al.,* 1983] and a few in the Antarctic [*Bromwich and Kurtz,* 1984; *Kottmeier and Engelbart,* 1992]. In wintertime the (upward) turbulent heat flux may reach 300-500 W m^{-2}, which is almost 2 orders of magnitude larger than the heat flux through the ice. Therefore even a small amount of open water or thin young ice formed on the lead or polynya surface may dominate the regional heat budget [*Maykut,* 1978]. In addition, the heat flux of the effective outgoing longwave radiation over polynyas in winter is of the order of 100 W m^{-2}. These heat fluxes influence sea ice formation and ocean stratification and thus the ocean circulation, as well as atmospheric stratification and circulation on a regional and even a global scale [*Ledley,* 1988; *Simmons and Budd,* 1991].

Since the gridlengths of large-scale atmospheric general circulation models (GCMs) are of the order of 200-500 km and those of numerical weather prediction models are about 40-100 km, the heat flux from leads and polynyas must be parameterized. The problem of parameterizing the surface fluxes over a heterogeneous surface has become one of the key issues in present-day research on the atmospheric boundary layer. In this context, partly ice-covered seas are in one sense simple, having no vegetation, no terrain height variations, no variations in surface moisture, and no extreme changes in surface roughness. In another sense they are more problematic than land surfaces, because subgrid variations in surface temperature can be extreme, even exceeding 30°C. The basic problem in the parameterization of turbulent heat fluxes is that we only know a single air temperature, surface temperature and wind speed for each grid square of a GCM. We can parameterize the surface fluxes solely on the basis of these grid-averaged variables, a method which we here call the mixture method. Alternatively, we can calculate local surface temperatures for the ice-covered and ice-free parts of the grid square (with the help of the radiation budget). The surface fluxes can then be calculated separately for the ice-free and ice-covered parts, the grid-averaged flux being some area average of these (the mosaic method). The basic questions are as follows: (1) What are reasonable values for the transfer coefficients? (2) How well do the grid-averaged air temperature, wind speed, and surface temperature (if the

Copyright 1995 by the American Geophysical Union.

Paper number 95JC02498.
0148-0227/95/95JC-02498$05.00

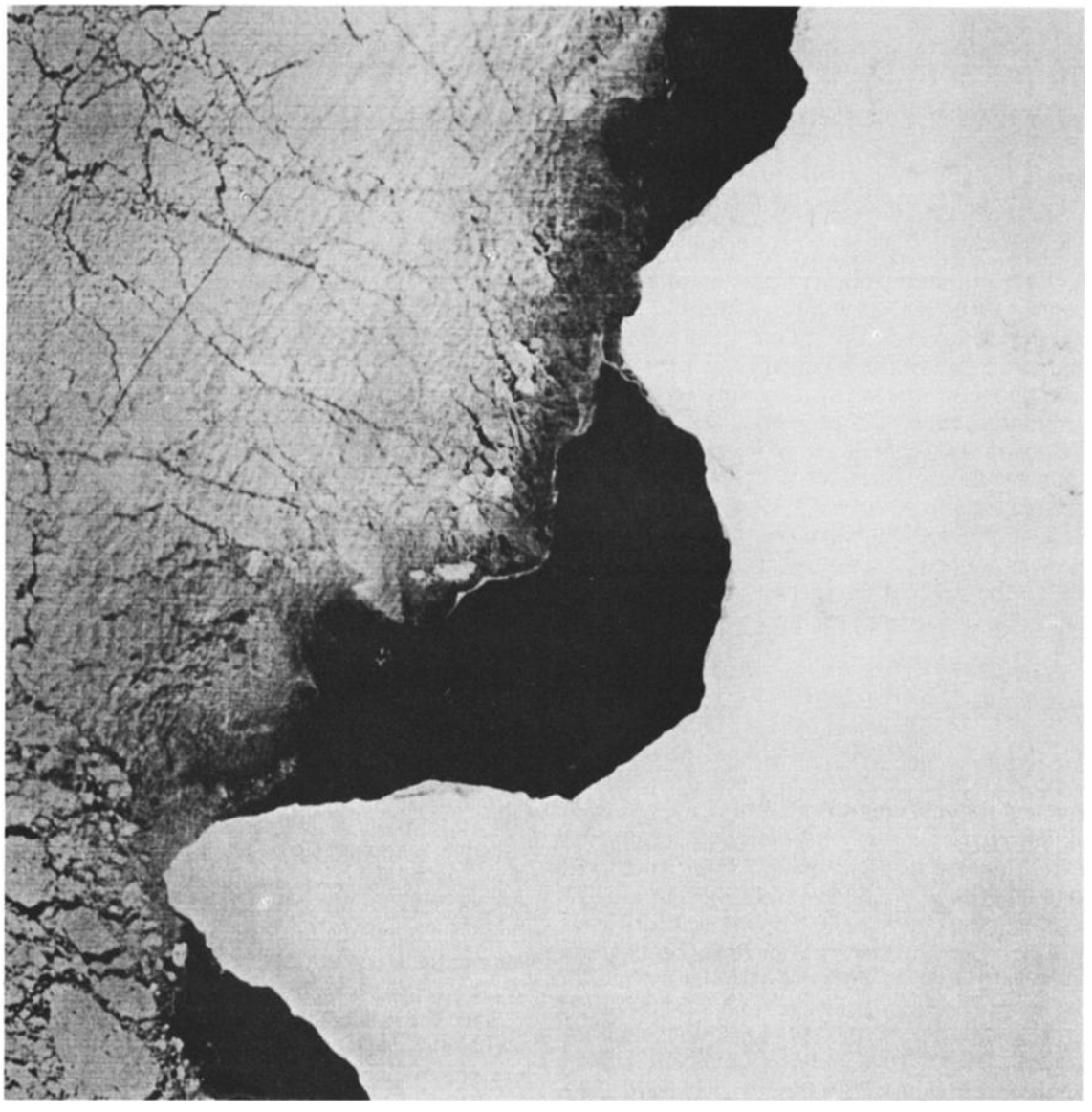

Figure 1. Landsat image showing part of the Laptev Sea Polynya (seen as a dark area) between regions of fast ice and fractured drifting ice. The size is 100x100 km, and the location is near 75°N, 137°E (the bright white, fast ice region includes parts of the snow-covered Belkovskiy and Kotelnyj Islands).

mixture method is used) represent the local values? If the leads are narrow, the air temperature and wind speed are not too much affected by the surface temperature variations, but in the case of wide polynyas the subgrid-scale variations between the ice-covered and ice-free parts of the grid square may be considerable. Parameterizing the radiative fluxes, problems arise from the subgrid variations in air temperature, cloudiness, and, if the mixture method is used, surface temperature and albedo.

From the point of view of modeling, ice margins create an analogous problem to polynyas, because the grid boundaries of GCMs do not coincide with the ice boundaries, resulting in large subgrid variations in surface temperature. This is also the case for tongues of open water in mostly ice-covered grid squares. For example, in wintertime the Barents Sea, Greenland Sea, Baffin Bay, and Davis Strait form such tongues (see *Gloersen et al.* [1992, p. 46-53] for a good illustration). Similar problems are encountered in coastal areas in autumn or early winter, when the sea is still open while the surface temperature over the land has already dropped. In addition to unbroken areas of warmer surface, series of polynyas may occur in the ice field, and the response of the atmospheric boundary layer may be different from the case of a single polynya.

Claussen [1991a] studied the surface heat flux parameterization on the scale of leads (10^1-10^3 m) and found relatively simple parametrization methods to work satisfactorily. In the present paper we concentrate on the scale of polynyas and simulate the airflow using a two-dimensional mesoscale planetary boundary layer (PBL) model. The model domain is intended to represent a single grid interval of a GCM. The approach is briefly introduced by *Vihma* [1994]. The results may naturally suffer from possible restrictions of the mesoscale model, but this is a reasonable way to test the parameterization schemes for GCMs when observations are lacking.

2. Parameterization Schemes

2.1. Turbulent Heat Fluxes

The simplest way to parameterize a grid-averaged turbulent surface heat flux from partly ice-covered sea is

$$\langle H\rangle = \rho_a c_p C_H^{\text{eff}}(\langle\theta_S\rangle-\langle\theta_Z\rangle)\langle V\rangle \quad (1a)$$

where angle brackets denotes a grid average, H is the turbulent sensible heat flux, ρ is the air density, and c_p is the specific heat. θ_S is the surface potential temperature (we assume through this paper that θ_S is a variable in a GCM, not specified, e.g., climatologically). θ_Z is the potential temperature of the air at height z. V is the wind speed, and C_H^{eff} is an effective heat transfer coefficient, for which we need to determine an appropriate value. Perhaps the simplest way is to use $\langle C_{HN}\rangle$, the area-average of neutral heat transfer coefficients over ice (C_{HN}^{i}) and over open water (C_{HN}^{w}). Then, $\langle H\rangle$ can be expressed in terms of local roughness lengths for momentum z_0 and temperature z_t

$$\langle H\rangle = \rho c_p\langle k^2[ln(z/z_0)]^{-1}[ln(z/z_t)]^{-1}\rangle(\langle\theta_S\rangle-\langle\theta_Z\rangle)\langle V\rangle \quad (1b)$$

where k is the von Karman constant = 0.4. A more sophisticated alternative, proposed by *Wood and Mason* [1991], is to express C_H^{eff} in terms of an effective roughness length for temperature Z_t^{eff}, which is analogous to that for momentum Z_0^{eff}

$$\langle H\rangle = \rho c_p k\langle u_*^2\rangle^{1/2}[ln(b/Z_t^{\text{eff}}) - \psi_H(b/L_m^{\text{eff}})]^{-1} \times(\langle\theta_S\rangle - \langle\theta_b\rangle) \quad (1c)$$

where b is the blending height, i.e., the approximate height at which the flow is independent of horizontal position and yet is still in equilibrium with the local surface (of course, these two conditions cannot be strictly valid at the same height). Here u_* is the friction velocity, L_m^{eff} is an effective Monin-Obukhov length, and ψ_H is a universal function describing the effect of stability on the temperature profile. The process which *Wood and Mason* [1991] present to determine $\langle u_*^2\rangle$, L_m^{eff}, and Z_t^{eff} is highly iterative, while practical use of (1c) in a GCM would require a simple yet accurate method of calculating Z_t^{eff}.

Both methods (1b) and (1c) describe the average heat flux as proportional to the average temperature profile $\langle\theta_S-\theta_Z\rangle$. This usually works, but because of the nonlinearity of heat flux with respect to the temperature profile, $\langle H\rangle$ may be the reverse of its normal direction relative to $\langle\theta_S-\theta_Z\rangle$ in certain conditions, as will be demonstrated in section 3, in which case the "mixture" parameterization schemes fail. It would be possible to add a correction term to $\langle\theta_S-\theta_Z\rangle$ expressed in terms of the fraction of the grid square that is covered by open water or the surface temperature variance. A universally valid functional form is, however, not easily found, and a more straightforward approach is to to use the mosaic technique to be presented next.

The mosaic method is based on the separation of the fluxes over the ice-covered and ice-free parts of the grid square. Following *Claussen* [1991a, b], we use the local transfer coefficients C_H^{i} and C_H^{w}, calculated at the blending height and depending on the local stratification. The method can be expressed as

$$\langle H\rangle = \rho c_p\langle V\rangle\langle C_H^{i,w}(\theta_S^{i,w}-\langle\theta_Z\rangle)\rangle = \rho c_p\langle V\rangle[fC_H^{w}(\theta_S^{w}-\langle\theta_Z\rangle) + (1-f)C_H^{i}(\theta_S^{i}-\langle\theta_Z\rangle)] \quad (2a)$$

where f is the open water fraction. Equation (2a) requires estimates for the surface temperature over the ice θ_S^{i} and water θ_S^{w}. There are several ways of calculating the local transfer coefficients. In keeping with the Monin-Obukhov similarity theory,

$$C_H^{i,w} = k^2[ln(b/z_0^{i,w}) - \psi_M(b/L^{i,w})]^{-1} \times[ln(b/z_t^{i,w})-\psi_H(b/L^{i,w})]^{-1} \quad (2b)$$

where ψ_M is the universal function describing the effect of stability on transfer of momentum. Like ψ_H, it depends on the stability parameter z/L (here b/L), where L is the (local) Monin-Obukhov length, which in turn depends on the fluxes of heat and momentum. In GCMs it is, however, impractical to determine L and H iteratively. L should therefore be calculated directly, e.g., from the Richardson number [*Large and Pond,* 1982; *Donelan,* 1982; *Andreas and Murphy,* 1986; *Launiainen,* 1995] or the transfer coefficients of, e.g., *Louis* [1979] could be used. The latter practice is adopted by *Stössel and Claussen* [1993] and the mosaic method is used, e.g., in the large-scale sea ice model of the Max-Planck-Institute in Hamburg, as well as in the GCM of the Main Geophysical Observatory in St. Petersburg. According to *Claussen* [1991a], (2b) should work for lead widths of the order of 10^1-10^2 m, and *Claussen* [1991b] showed that (2b) is applicable, even when there are strong subgrid variations in surface roughness. A practice comparable to the mosaic method is used in data analyses to calculate areally averaged fluxes over fractured sea ice cover [*Andreas and Makshtas,* 1985; *Launiainen and Vihma,* 1994].

If more accuracy is needed, the idea of local parameterization can be developed further. In addition to local transfer coefficients, we can calculate estimates of local wind speed and air temperature on the basis of the GCM's $\langle V\rangle$, $\langle\theta_Z\rangle$, $\langle\theta_S^{i}\rangle$, and $\langle\theta_S^{w}\rangle$. V and θ over ice and over water ($V_0^{i,w}$, $\theta_0^{i,w}$) can be found using the stability-corrected logarithmic profiles:

$$V_0^{i,w} = (u_*^{i,w}/k)\,ln[b/z_0^{i,w} - \psi_M(b/L^{i,w})]$$
$$\theta_0^{i,w} = \theta_S^{i,w} + \theta_*^{i,w}\,ln[b/z_t^{i,w} - \psi_H(b/L^{i,w})]$$

where $\theta_*^{i,w} = -H^{i,w}/(\rho c_p k u_*^{i,w})$. First, $H^{i,w}$ and $u_*^{i,w}$ are computed from $\langle\theta_Z\rangle$, $\langle V\rangle$, and $\theta_S^{i,w}$ using the Monin-Obukhov theory with L depending on the Richardson number (proportional to $\langle\theta_Z\rangle$, $\langle V\rangle$, and $\theta_S^{i,w}$). Then, we calculate $\theta_*^{i,w}$ and further $V_0^{i,w}$ and $\theta_0^{i,w}$. The above would, however, mean that the wind speed and air temperature adjust immediately to the changed surface conditions, which is not the case. To account for the dependency on fetch and height in the modification, one can take a weighted average of the grid-averaged values and the values representing local equilibrium

$$V^{i,w} = g_V V_0^{i,w} + (1-g_V)\langle V\rangle$$
$$\theta^{i,w} = g_\theta \theta_0^{i,w} + (1-g_\theta)\langle\theta\rangle \quad (3)$$

where $0 < g_V, g_\theta < 1$. The optimal values for g_V and g_θ depend on the situation, but if (3) is applied at the blending height,

$g_\theta = g_V = 0.5$ could be used as a basic estimate, because that represents an even mixture of local equilibrium and horizontal homogeneity. After computing $V^{i,w}$ and $\theta^{i,w}$ we can calculate $\langle H \rangle$ from (4). The process could, of course, be iterated further, but this is impractical in GCMs.

$$\langle H \rangle = \rho c_p [f C_H^w V^w (\theta_S^w - \theta_Z^w) + (1-f) C_H^i V^i (\theta_S^i - \theta_Z^i)] \quad (4)$$

The above (formulas (1a) to (4)) holds for the turbulent latent heat flux λE as well, if we just replace θ by the specific humidity q and c_p by the latent heat of sublimation λ. According to the present knowledge, the transfer coefficients and roughness lengths for humidity are either equal or at least close to those for heat [e.g. *Schmitt et al.*, 1979; *Andreas*, 1987; *Smith*, 1989]. We will use (1a) to (4) to parameterize $\langle H \rangle$ and $\langle \lambda E \rangle$ on the basis of $\langle V \rangle$, $\langle \theta_Z \rangle$, θ_S^i and θ_S^w obtained from a two-dimensional model.

2.2. Radiative Fluxes

Almost the same problems that are encountered in the parameterization of turbulent heat fluxes are also present when parameterizing the radiation balance of the surface. In the case of incoming solar (shortwave) radiation, the subgrid variations in albedo and cloudiness should be considered. If we can estimate representative values for albedo and cloudiness (if there are systematic variations in the latter) for the ice-covered and ice-free parts of the grid square (α^i, α^w, N^i, and N^w, respectively), a mosaic method should work for the grid-averaged broadband shortwave radiation flux $\langle Q_S \rangle$:

$$\langle Q_S \rangle = f(1-\alpha^w) Q_{0S} \varphi(N^w) + (1-f)(1-\alpha^i) Q_{0S} \varphi(N^i) \quad (5)$$

where Q_{0S} is the incoming shortwave radiation flux in cloud-free conditions and $\varphi(N)$ is a reduction factor depending on cloudiness.

Considering the longwave radiation, the quantity we should determine is the grid average of the surface net longwave radiation Q_L, which depends on the air and surface temperatures and on emissivity, air moisture, and cloudiness. The problem resembles that of turbulent heat fluxes, but the dependence on wind speed is replaced by that on cloudiness. We look at the possibilities for grid averaging on the basis of the empirical formula by *Maykut and Church* [1973]. In low temperatures there is a lot of scatter between the results from the various empirical formulas for Q_L, but the above reference was recommended on the basis of an extensive Russian data set (A. Makshtas, personal communication, 1994). The mixture technique would give for $\langle Q_L \rangle$

$$\langle Q_L \rangle = -0.97\sigma \langle T_S \rangle^4 + (0.7855 + 0.2232 \langle N \rangle^{2.75}) \sigma \langle T_Z \rangle^4 \quad (6)$$

Adopting the mosaic technique for T_S results in

$$\langle Q_L \rangle = f[-0.97\sigma (T_S^w)^4 + (0.7855 + 0.2232 \langle N \rangle^{2.75}) \sigma \langle T_Z \rangle^4] + (1-f)[-0.97\sigma (T_S^i)^4 + (0.7855 + 0.2232 \langle N \rangle^{2.75}) \sigma \langle T_Z \rangle^4] \quad (7)$$

In atmospheric GCMs the computation of longwave radiation is a far more complex process, but in many sea ice models a simple parameterization like (6) is applied. Modifications to formulas (6) and (7) can be developed, as in the case of turbulent heat fluxes. One possibility would be to go further and separate the air temperature and cloudiness analogously to (4). As Q_L changes slowly with temperature, the separation of cloudiness into N^i and N^w is, however, more important, if it can be done reliably.

2.3. Momentum Flux

The turbulent surface momentum flux over an ice-covered ocean depends on skin drag and on form drag, as stated by the drag-partition theory [*Marshall*, 1971; *Arya*, 1975]. The form drag arises from floe edges, pressure ridges, and patterns of snowdrift. In the mesoscale model used for the present study, we cannot explicitly resolve the form drag from such small surface features. We set a value of 1 mm for the ice roughness length, which merely represents the effect of skin drag. We could parameterize the total wind drag on the basis of a given distribution of floe size, freeboard, and ridging [*Hanssen-Bauer and Gjessing*, 1988; *Stössel and Claussen*, 1993]. Parameterization schemes for a hypothetical GCM including the effect of form drag could not, however, be verified by the mesoscale model. Therefore we only discuss the problem of parameterizing the skin drag, denoted as τ.

The problems are basically similar to those with the heat flux. We can use an effective drag coefficient and the grid-averaged wind speed. The simplest possibility is to calculate the stability correction ψ_M from the grid averages $\langle \theta_Z \rangle$, $\langle \theta_S \rangle$, and $\langle V \rangle$. Thus an effective drag coefficient C_D^{eff} is calculated as an area average on the basis of local roughness lengths and "mixture" ψ_M:

$$\langle \tau \rangle = \rho C_D^{\text{eff}} \langle V \rangle^2 = \rho \langle k^2 / [\ln(z/z_0^{i,w}) - \psi_M]^2 \rangle \langle V \rangle^2 \quad (8)$$

Separating T_S over ice and water to get ψ_M^i and ψ_M^w yields

$$\langle \tau \rangle = \rho \langle k^2 / [\ln(z/z_0^{i,w}) - \psi_M^{i,w}]^2 \rangle \langle V \rangle^2 \quad (9)$$

The separation can again be developed further by calculating a local air temperature and wind speed for the ice-covered and ice-free parts according to (3) and then applying an equation analogous to (4). A combination of an effective roughness length Z_0^{eff} and separated $\psi_M^{i,w}$ can be used as well.

$$\langle \tau \rangle = \rho \langle k^2 / [\ln(z/Z_0^{\text{eff}}) - \psi_M^{i,w}]^2 \rangle \langle V \rangle^2 \quad (10)$$

Z_0^{eff} can be obtained from *Taylor's* [1987] formula as follows: $\ln(Z_0^{\text{eff}}) = \langle \ln(z_0) \rangle + 0.09\sigma^2_{\ln(z0)}$, where $\sigma^2_{\ln(z0)}$ is the variance of local roughness lengths in the grid square, or from *Mason's* [1988] formula: $\{\ln[L_c/(200 Z_0^{\text{eff}})]\}^{-2} = \langle \{\ln[L_c/(200 z_0)]\}^{-2} \rangle$, where L_c is the fetch over a homogeneous surface section.

Wood and Mason [1991] preferred to use a mixture for both the roughness length and ψ_M function yielding the form

$$\langle \tau \rangle = \rho k^2 \langle [\ln(b/Z_0^{\text{eff}}) - \psi_M]^{-2} \rangle \langle V \rangle^2 \quad (11)$$

Taylor [1987] derived his a forementioned equation for Z_0^{eff} from an idea of computing regional roughness from a geostrophic drag coefficient $C_G = u_*/G$, where G is the geostrophic wind speed. Another possibility is to keep using C_G and parameterize $\langle \tau \rangle$ on the basis of the surface pressure field, i.e., the geostrophic wind.

$$\langle \tau \rangle = \rho C_G^2 G^2 \quad (12)$$

Over polar oceans, very little verification data are available for the actual surface wind. The pressure field is thus more reliably known for a GCM, and the problem is to determine the geostrophic drag coefficient. *Overland and Davidson* [1992] and *Overland and Colony* [1994] estimated C_G over the Arctic sea ice on the basis of field data, and the results showed an apparent dependence on the atmospheric stability, but the stability conditions over grid squares containing a large fraction of open water are out of the range of the field data. Thus a representative value for C_G to be used in the present study is uncertain, but we shall first try to estimate C_G using the mesoscale model results.

2.4. Vertical distribution of heat

In addition to the problem of parameterizing the horizontal area averages, the vertical distribution of heat should be considered. The subgrid-scale upward transport of heat results partly from turbulent diffusion and partly from mesoscale circulations. The field experiments of, e.g., *Schnell et al.* [1989] and *Dethleff* [1994] showed that buoyant heat plumes originating from leads or polynyas may reach altitudes of several kilometers penetrating through the polar inversion. This is problematic for many GCMs, because the usual practice is that the subgrid-scale heat flux is released into the lowest model layer. Thus the vertical heat transfer would be underestimated, and the amount of heat returned to the ice would be overestimated. A typical height for the lowest model level in GCMs is of the order of 100 m or below that; e.g., in the 31-level model of the European Centre for Medium-Range Weather Forecasts the three lowest levels are at approximately 30, 150, and 350 m. Even a denser vertical grid could not resolve the plumes because of their small horizontal extent. *Glendening and Burk* [1992] studied the flow over a lead 200 m wide using a large-eddy simulation model and gave an equation for the maximum plume height Z_p

$$Z_p = (Q_s W^2/V\gamma)^{1/3} \tag{13}$$

where $Q_s = Hw/\rho c_p$, W is the lead width, and $\gamma = \partial\theta/\partial z$ upwind of the lead. *Serrezze et al.* [1992] developed an equation to predict the maximum temperature that air flowing over a lead can reach. Using this predicted temperature and sounding data, they studied the theoretical heights of buoyant convection. The theoretical height for a plume associated with a 1-km-wide lead was 985 m. A higher plume rise would require light winds, a low surface temperature, and a weak low-level temperature inversion, a combination atypical of the Arctic, and conditions favoring a high plume rise do not favor the formation of large leads [*Serrezze et al.*, 1992]. The result of 985 m is, however, already far above a typical GCM's lowest level.

Although wide polynyas should be rare in the central Arctic, they are more common in the generally divergent field of Antarctic sea ice and are potential origins for high plume rises. In section 5 we try to simulate the vertical distribution of heat originating from large polynyas.

3. Theoretical Examples

In the case of narrow leads, simple considerations about the area averaging may be made, assuming that the leads are so narrow that the wind speed is not affected and the temperature of the air mass flowing from over the ice to over the lead does not change significantly. θ_Z does change, of course, but the change should remain small relative to the temperature difference θ_S-θ_Z. Accordingly, the local heat flux could be calculated using $\langle\theta_Z\rangle$ as a local $\theta_Z^{i,w}$ and $\langle V\rangle$ as $V^{i,w}$. In this case the mosaic method of (2a) should work, if applied at the blending height. If a lower reference height is used for calculations, the air mass modification may be important, particularly on horizontal scales of tens of meters, as shown by *Worby and Allison* [1991]. The mosaic method could, however, probably work relatively well also with reference heights lower than the blending height, because the integral effect of modification is felt in $\langle\theta_Z\rangle$. Therefore $\langle\theta_Z\rangle$ gives too small a flux over the ice and too large a flux over the lead. These compensate each other, though not completely, because the heat flux is nonlinearly proportional to θ_S-θ_Z. The situation becomes more complicated when the lead is wide enough to modify the wind field.

We now examine whether the mixture method (1a) is, in principle, applicable for the parameterization of $\langle H\rangle$. Assuming certain values of wind speed, air temperature, and surface temperature for ice and open water and 10 m as the blending height, we calculate the local H and local C_H over ice and over leads using the algorithm of *Launiainen and Vihma* [1990]. Then we get $\langle H\rangle$ and $\langle C_H\rangle$ for arbitrary lead coverage and solve C_H^{eff} from (1a). We take the following two examples: (a) unstable stratification over the sea ice, $V_{10m} = 10\ \text{m s}^{-1}$, $\theta_S^w = -1.8°\text{C}$, $\theta_S^i = \theta_{10m} + 2°\text{C}$, (b) stable stratification over the sea ice, $V_{10m} = 10\ \text{m s}^{-1}$, $\theta_S^w = -1.8°\text{C}$, $\theta_S^i = \theta_{10m} - 2°\text{C}$. The resulting ratio of $C_H^{\text{eff}}/\langle C_H\rangle$ with respect to θ_{10m} is presented in Figure 2. We see that in the case of unstable stratification, C_H^{eff} is always close to $\langle C_H\rangle$ (Figure 2a) and (1a) is thus appropriate to parameterize $\langle H\rangle$. We only need to determine C_H^{eff}. In stable stratification, however, the ratio $C_H^{\text{eff}}/\langle C_H\rangle$ is well behaved only when the lead coverage remains sufficiently small (Figure 2b). For larger fractions of open water, countergradient fluxes are encountered, seen as negative C_H^{eff}. An example is given in Figure 2c, where a 10% lead coverage leads to a countergradient flux when $-21°\text{C} < \theta_{10m} < -20°\text{C}$. When $\langle\theta_S - \theta_{10m}\rangle$ goes to zero, a finite C_H^{eff} cannot produce the correct $\langle H\rangle$.

If the correct direction of heat flux is considered to be of primary importance, the simple form (1a) is safe to use only in cases of unstable stratification over sea ice. Such cases occur over thin ice with a large heat flux from the ocean through the ice [*Worby and Allison*, 1991], but a more typical situation over sea ice is stable stratification [e.g., *Makshtas*, 1991]. The absolute error due to countergradient fluxes remains small, however, because the grid-averaged flux is small in such cases.

4. Mesoscale Model

The airflow over polynyas was simulated using a two-dimensional hydrostatic mesoscale planetary boundary layer model. The flow is forced by a large-scale pressure gradient represented by the geostrophic wind. The model has an (x,σ) coordinate system with 62 grid points in the horizontal and 10 in the vertical at the approximate heights of 2, 10, 30, 50, 100, 200, 350, 600, 1100, and 2000 m. The upper boundary condition is applied at 3 km, where the wind

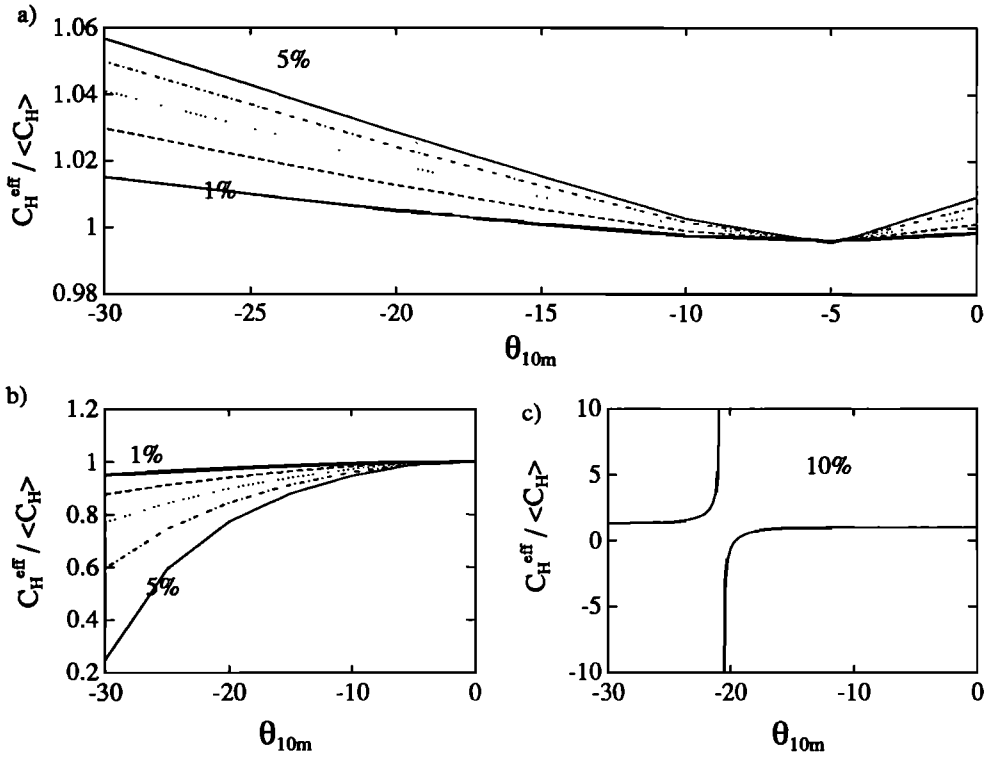

Figure 2. Effective heat transfer coefficient C_H^{eff} with respect to the true area average of C_H as a function of air temperature with (a) unstable stratification, $\theta_S^i = \theta_Z^i + 2°C$; lead coverage, 1-5% and (b) stable stratification, $\theta_S^i = \theta_Z^i - 2°C$; lead coverage 1-5%, and (c) stable stratification as in Figure 2b, but for lead coverage of 10%.

becomes geostrophic (a couple of control runs were made using a 50-level version of the model extending up to 6 km; see section 6.2). All fluxes vanish at the horizontal boundaries, and the vertical velocity vanishes at the top (3 km) and bottom. In the present experiments the grid length was 2 km with flat topography. Vertical diffusion is solved by an implicit method, and instead of explicit horizontal diffusion, a weak low-pass filter is applied to all fields. The model equations and details are given by *Alestalo and Savijärvi* [1985]. The main modifications to the model for the present study were an inclusion of the air moisture and a development of the surface layer description by incorporating an iterative Monin-Obukhov scheme instead of the original *Louis* [1979] type of transfer coefficients. In the Ekman layer, turbulence is described by first-order closure with the vertical diffusion coefficient $K = l^2 (dU/dz) f(Ri)$, where the mixing length $l = kz/(1+kz/\varepsilon)$, ε = 30 m. Here $f(Ri)$ is an empirical function depending on the Richardson number. In unstable stratification, $f(Ri) = (1\text{-}16Ri)^{1/2}$ for momentum and $f(Ri) = (1\text{-}64Ri)^{1/2}$ for heat and moisture. In stable stratification, max(0.1, 1-5*Ri*) is used for momentum, heat, and moisture.

Over water the surface temperature is kept at the freezing point of -1.8°C. Over ice the surface temperature change is calculated from the energy balance determined by the turbulent fluxes of sensible and latent heat, the incoming shortwave radiation (zero in the winter experiments), the net longwave radiation Q_L, and the heat flux through ice and snow S. We calculate Q_L from the empirical formula by *Maykut and Church* [1973]. In calculating S, we assume a linear temperature profile in the ice and snow, which should be reasonable, because the model is run into a steady state before analyzing the results. The experiments and the initial and boundary conditions used are shown in Tables 1a and 1b. A polar inversion with dT/dz = 1 K km^{-1} is used as the initial

Table 1a. Model Experiments

Simulation	Description
Group 1	one polynya, seven runs; f = 0, 0.1, 0.3, 0.5 0.7, 0.9, and 1; G perpendicular to the ice edge
Group 2	same as 1, but G parallel to the ice edge
Group 3	same as 1, but an ice patch replacing the polynya
Group 4	f = 0.5; four runs; number (and width) of polynyas as follows: 1 (60 km), 3 (20 km), 6 (10 km), and 10 (6 km); G perpendicular to the ice edge
Group 5	same as 4, but G parallel to the ice edge
Group 6	f = 0.5, single ice edge; a, on-ice G; b, off-ice G; c, G parallel to the ice edge

Here f is the open water fraction and G is geostrophic wind speed.

Table 1b. Initial and Boundary Conditions for Model Experiments on July 1 at 70°S

Variable	Value
Snow surface temperature T_S^i, °C	-33
Water surface temperature T_S^w, °C	-1.8
Geostrophic wind G speed m s^{-1}	10
ice roughness length z_0^i, mm	1
water roughness length z_0^w, mm	≅0.05*
temperature profile dT/dz, K km^{-1}	1†
relative humidity RH, %	90
snow depth, m	0.2
ice thickness, m	0.7
heat conductivity of ice, W m^{-1} K^{-1}	2.1
heat conductivity of snow, W m^{-1} K^{-1}	0.3

* Value is wind dependent.
† Value was -6.5 in group 3.

temperature profile, and the initial wind profile is given as an Ekman-Taylor spiral.

While calculating the turbulent fluxes by the Monin-Obukhov theory, we describe the stability effects using the universal functions of *Högström* [1988] in unstable cases and those of *Holtslag and de Bruin* [1988] in stable cases. The (local) roughness length for momentum is set to 1 mm over ice, and over water it is calculated from the wind speed according to *Smith* [1980]. The (local) roughness lengths for heat and moisture are calculated according to *Andreas* [1987] over ice and according to *Launiainen* [1983] over water. Details of the surface layer parameterizations are given by *Launiainen and Vihma* [1990].

This model has been used previously in several studies of mesoscale circulation systems both for the Earth and for Mars [e.g., *Savijärvi and Siili,* 1993]. *Savijärvi* [1991] validated the model against an extensive boundary layer data set both in convective and stable conditions.

5. Simulations

5.1. Experiments

The 2-D PBL model was used to simulate flow associated with long polynyas, 6-108 km wide. The whole model domain (124 km) was considered as representing a single grid square of a hypothetical GCM. The grid points of the mesoscale model (2 km apart) were set to be either totally ice covered or totally ice free without any subgrid size leads or ice patches. Thus we did not have to apply any of the methods (1a) to (4) to parameterize $\langle H \rangle$ in the model but used the model results as a reference against (1a) to (4).

The model was run for 96 hours (if not otherwise mentioned) to reach a steady state after a weak initial inertial oscillation had damped down and the boundary layer over a polynya had fully developed. We concentrated on the polar (Antarctic) winter case with extreme differences between the surface temperature of ice and polynya (Table 1b). In the first experiments a geostrophic wind with a speed of $G = 10$ m s^{-1} is blowing across the polynya. The polynya, located in the middle of the model domain, has a width varying from 6 to 108 km. The PBL over the polynya is very unstable. Simulations were run with $f = 10$, 30, 50, 70, and 90% of open water in the area, as well as the reference cases of a totally ice-covered ($f = 0$%) and a totally ice-free ($f = 100$%) model domain.

In the next stage we allowed the geostrophic wind to blow parallel to the polynya. Simulations were made with the same fractions of open water and the same initial and boundary conditions as before. The third group of simulations was made having ice in the middle of the domain using the same fractions of open water. The latter runs resulted in a stably stratified PBL as a warm air mass from the open sea was advected over the cold ice surface. The fourth group was made by varying the number of polynyas, the model domain containing 50% open water in each case; in addition to the former run with one polynya and a 50% open water fraction, the model was run with 3, 6, and 10 polynyas, each of them being 20, 10, and 6 km wide, respectively. The geostrophic wind was perpendicular to the polynyas. The fifth group was the multipolynyas case but with the geostrophic wind parallel to the polynyas. In the fourth and fifth groups the horizontal grid of the model was extended to 82 x 2 km in order to prevent disturbances arising from changes in the surface type too close to the inflow boundary (the results were analyzed from the 60 grid points in the middle of the domain, as in the other simulations). Finally, we modeled the flow over a single ice edge in the middle of the model domain using different directions of G. The simulations are summarized in Tables 1a and 1b.

5.2. Flow properties

5.2.1. Single polynya (group 1 simulations). The general flow properties from the simulations with the polynya in the middle of the model domain are presented in Figure 3, where we take the case with 50% open water as an example. The surface layer results are comparable to field data for that latitude and season [*Kottmeier and Hartig,* 1990; *Launiainen and Vihma,* 1994], although the air and surface temperatures over the ice are somewhat lower than the observed mean values, because large-scale heat advection was lacking from the mesoscale model. The air temperature (Figure 3a) at 2 m increased over the polynya by approximately 0.1°C/km. The rise of air temperature was naturally largest at the lowest levels, as was also its decrease downwind of the polynya, because of recapture of heat by the ice. For example, in the case of a 50% open sea fraction the maximum warming was 6.6°C at a height of 2 m, while it was 4.2°C at a height of 100 m. Yet the temperature increase between the first and last grid point was the same, 4.1°C, at both levels. The behavior of specific humidity (Figure 3b) resembled that of air temperature, except that q_S exceeded q_Z over the ice as well.

The near-surface wind speed (Figure 3c) nearly doubled over the polynya (see section 5.7 for the reasons). The PBL was very unstable over the polynya, and the surface sensible heat flux H reached 520 W m^{-2}, the latent heat flux λE reached 160 W m^{-2}, and the net outgoing longwave radiation Q_L reached 90 W m^{-2} (Figure 3d). Over the sea ice upstream of the polynya, stratification was stable, with a sensible heat flux H of -14 W m^{-2}. Over the ice downstream of the polynya, stratification was even more stable due to warming of the air mass, and H had a minimum of -22 W m^{-2}. The variations in the longwave radiation over the polynya in Figure 3d (reflected also in the surface temperature and sensible heat flux)

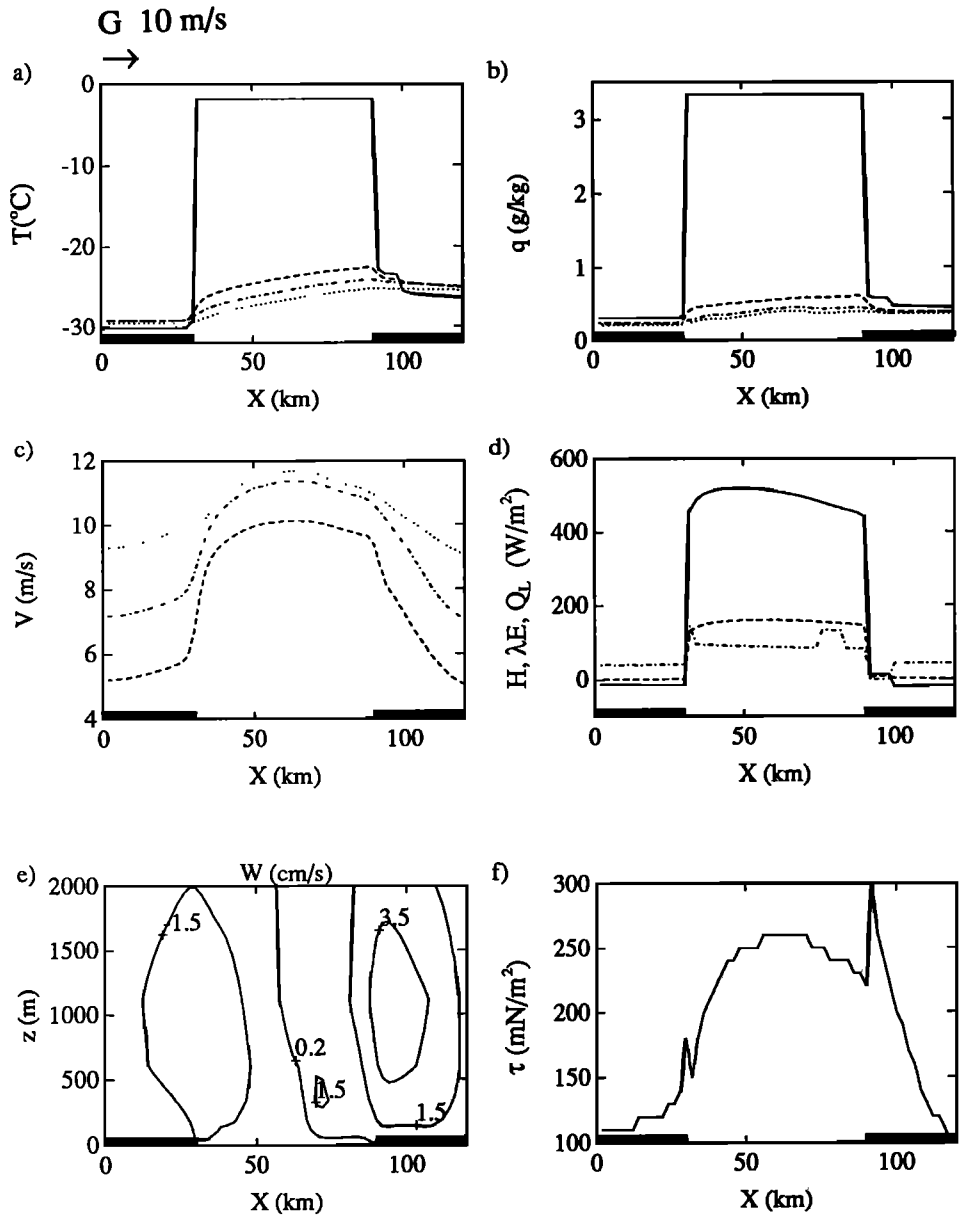

Figure 3. Flow properties in the case of one polynya in the middle of the ice field with a 50% open water fraction and G perpendicular to the ice edges. The location of ice is marked by the thick line in the X axis. (a) Surface temperature (solid line) and air temperature at heights of 2 m (dashed line), 30 m (dot-dashed line), and 100 m (dotted line). (b) Surface specific humidity (solid line) and specific humidity in the air at heights of 2 m (dashed line), 30 m (dot-dashed line), and 100 m (dotted line). (c) Wind speed at heights of 2 m (dashed line), 30 m (dot-dashed line), and 100 m (dotted line). (d) Turbulent surface fluxes of sensible (solid line) and latent (dashed line) heat and the net longwave radiation at the surface (dot-dashed line). (e) Cross section of vertical velocity. (f) Surface momentum flux.

were due to variations in cloudiness; a grid point in the mesoscale model is either cloud covered or cloud free (the effect is even more pronounced in Figure 4). The field of vertical velocity w was interesting, with a rising motion of 5 cm s^{-1} over the ice downwind of the polynya (Figure 3e). The maximum resulted primarily from stability effects at the ice edge: the heated air rose over the stable surface layer above the ice, as in a synoptic-scale warm front. The roughness change was less important for w. Because of the dramatic change in stability and increase in surface wind speed, the surface momentum flux (Figure 3f) was larger over the polynya than over the ice, although the roughness was higher over the ice. The edges of the polynya induced spikes in the momentum flux, because z_0 changes immediately but the wind speed does not.

5.2.2. Single polynya with parallel wind (group 2). When the geostrophic wind blew parallel to the ice edge (Figure 4), the fields of air temperature and humidity, horizontal wind speed, and turbulent surface fluxes did not differ drastically from the cases with a perpendicular wind. Yet the air temperature was 13-16°C higher and the turbulent heat fluxes over the polynya therefore smaller. Because of surface friction, the near-surface wind deviates 15-20° to the left of the geostrophic wind, and this tends to produce a weak wind

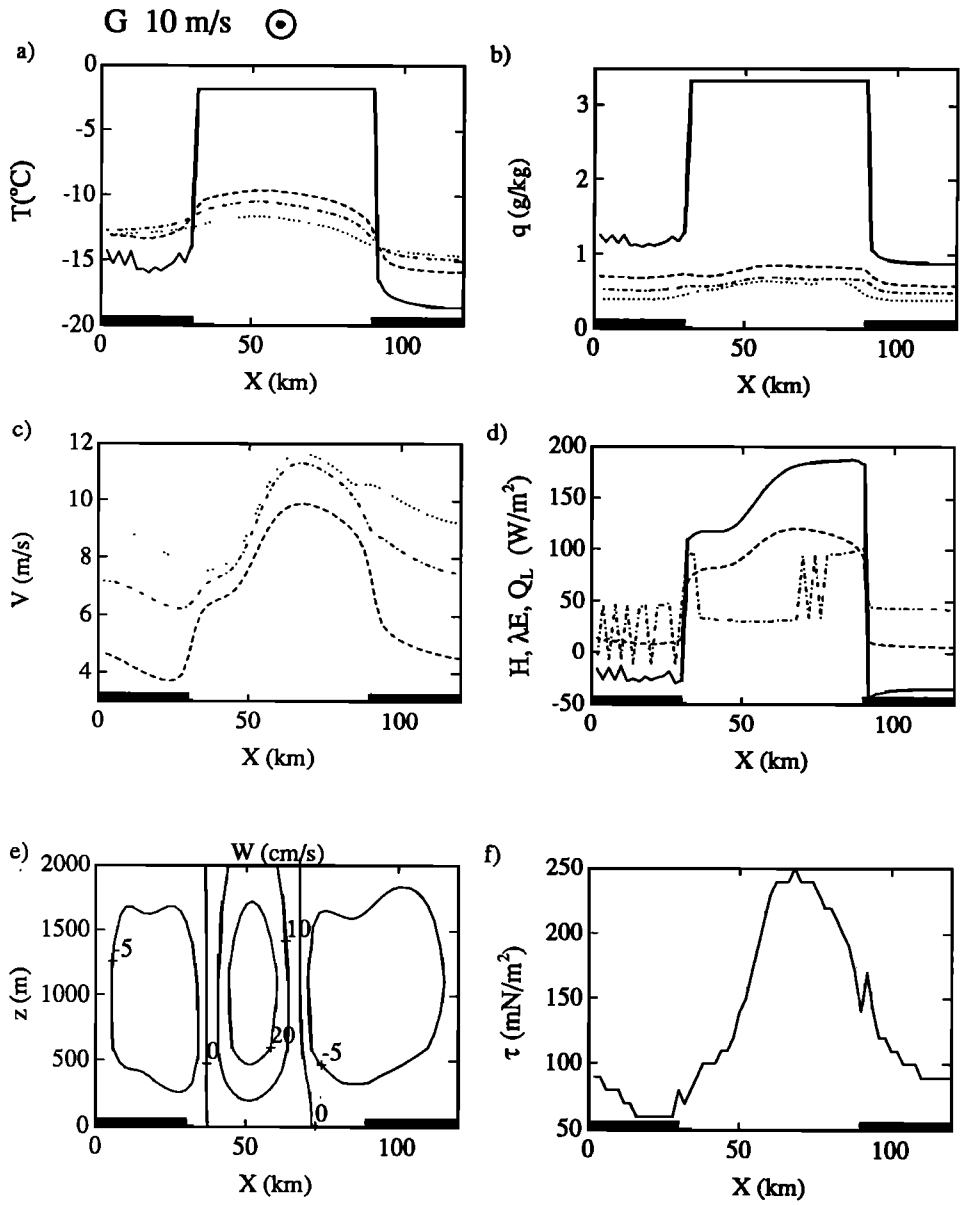

Figure 4. Flow properties in the case of one polynya in the middle of the ice field with a 50% open water fraction and G parallel to the ice edges. The location of ice is marked by the thick line in the X axis. (a) Surface temperature (solid line) and air temperature at heights of 2 m (dashed line), 30 m (dot-dashed line), and 100 m (dotted line). (b) Surface specific humidity (solid line) and specific humidity in the air at heights of 2 m (dashed line), 30 m (dot-dashed line), and 100 m (dotted line). (c) Wind speed at heights of 2 m (dashed line), 30 m (dot-dashed line), and 100 m (dotted line). (d) Turbulent surface fluxes of sensible (solid line) and latent (dashed line) heat and the net longwave radiation at the surface (dot-dashed line). (e) Cross section of vertical velocity. (f) Surface momentum flux.

component across the polynya (v_{2m} ~ 2 m s^{-1}). This is the reason for the asymmetry in Figure 4. The cross-polynya component was not uniform, however, even changing the wind direction. This was because the surface temperature gradient induced strong secondary circulations, with a maximum vertical velocity of from 10 to 31 cm s^{-1} and an associated cross-polynya wind component (e.g., v_{2m} varied from -4.1 m s^{-1} at X = 70 km to 2.2 m s^{-1} at X = 38 km; compare Figure 4). The intense updraft area is seen in the surface layer as a maximum of air temperature but as locally reduced values of horizontal wind speed and turbulent surface fluxes. The mesoscale cell grew in strength during the first 72 hours of simulation, but it transferred heat horizontally and diminished the surface temperature difference between the ice and the polynya. Thus the cell destroyed its own driving force and became gradually less intense, with only 1-3 cm s^{-1} maximum updrafts after 192 hours of simulation. For this reason we did not run the model to a steady state in these simulations. The steady state would not represent a wintertime temperature contrast and would require the wind direction to have remained constant for almost 10 days, which is unrealistic for most high-latitude sites (except, perhaps, for katabatic winds, but they are not normally parallel to polynyas). Moreover, if the ice could drift freely with the

wind, the polynya would be closed in such a time (assuming an approximately 3% drift ratio and 20-30° turning angle). As a result, we analyzed the model fields after 72 hours of integration, which represents the maximum strength of the mesoscale circulations.

The maximum vertical velocity in the mesoscale cell depends not only on the simulation time, but also on the grid length used, the maximum values after 72 hours being 28, 20, and 13 cm s^{-1} with respective grid lengths of 2, 4, and 6 km. This is mainly because the intense updraft area is narrow, although the hydrostatic assumption also may overestimate vertical velocities for relatively small grid lengths. The simulations with different grid lengths yielded otherwise similar results.

5.2.3. Ice patch (group 3). Figure 5 shows results from runs with ice in the middle (with G perpendicular to the ice edge). The initial temperature profile was now dT/dz = -6.5 K km^{-1} corresponding to the open-ocean conditions at the inflow boundary. Now the PBL over the open water is near neutral and becomes stable over the cold ice. The air temperature (2 m) diminishes toward the downwind edge of the ice patch by only 4°C, while the wind speed is reduced to almost half. For two reasons the modification in air temperature is now smaller than in the case with a polynya surrounded by ice. First, in the stable conditions the turbulent fluxes are smaller, and second, even the relatively small downward heat flux (Figure 5d) is able to affect the snow surface temperature, while in the polynya case the water

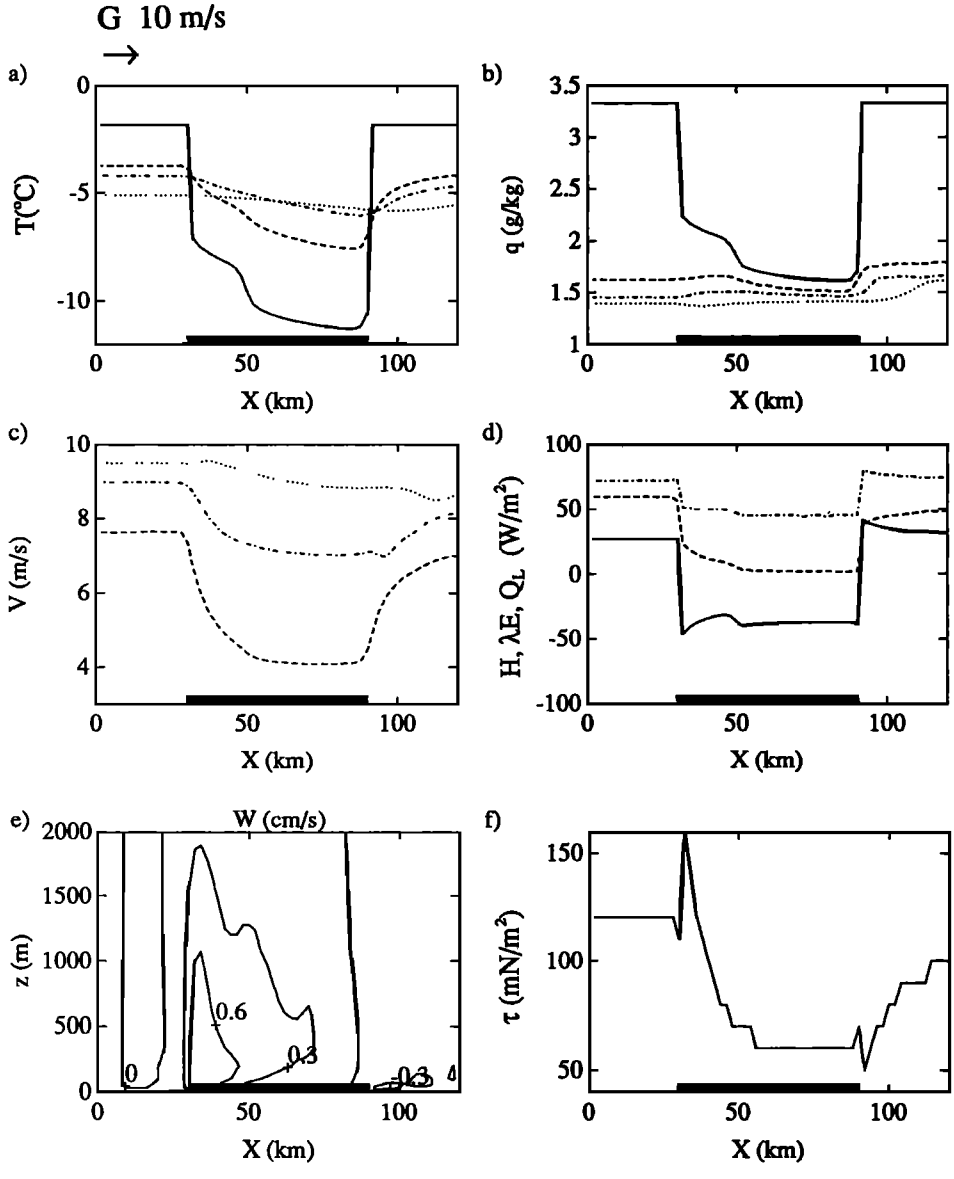

Figure 5. Flow properties in the case of a single ice patch surrounded by open ocean, 50% open water fraction. The location of ice is marked by the thick line in the X axis. (a) Surface temperature (solid line) and air temperature at heights of 2 m (dashed line), 30 m (dot-dashed line), and 100 m (dotted line). (b) Surface specific humidity (solid line) and specific humidity in the air at heights of 2 m (dashed line), 30 m (dot-dashed line), and 100 m (dotted line). (c) Wind speed at heights of 2 m (dashed line), 30 m (dot-dashed line), and 100 m (dotted line). (d) Turbulent surface fluxes of sensible (solid line) and latent (dashed line) heat and the net longwave radiation at the surface (dot-dashed line). (e) Cross section of vertical velocity. (f) Surface momentum flux.

temperature is not changed (see also *Brümmer et al.* [1994]). Owing to stability effects, the momentum flux over the ice is reduced to half of its value over the ocean. This agrees with the observations of *Fairall and Markson* [1987] in the Marginal Ice Zone Experiment.

5.2.4. Many polynyas (groups 4 and 5). The distributions of air temperature and wind speed resulting from simulations with a varying number of polynyas are presented in Figure 6. In cases with G perpendicular to the ice edges we note that the amplitude of the variations in air temperature and wind speed decreases with an increasing number of polynyas. The modification in air temperature (10 m) across one polynya with respect to the surface temperature change ($\delta\theta_{10m}/\delta\theta_S$) decreases from the 0.20 of the single-polynya case down to the 0.04 of the 10-polynya case, but the total warming over the model domain remains the same. The pattern of surface wind speed (Figure 6b) resembles that of air temperature, except that the wind speed adjusts to the new conditions faster than air temperature. The grid-averaged wind speed is not especially sensitive to the number of polynyas. When G was set parallel to the ice edges, the temperatures were much higher. The asymmetry is again due to the wind component across the polynya. The distribution of surface heat fluxes appeared as square waves, as in Figures 3d and 4d.

We already saw from Figure 4e that the geostrophic wind parallel to the ice edges resulted in vigorous secondary circulations with strong updrafts and downdrafts. With parallel G the maximum updrafts were strongly reduced with increasing number (decreasing width) of polynyas, being 27.8, 24.5, 13.6, and 10.5 cm s^{-1} for 1, 3, 6, and 10 polynyas, respectively. With perpendicular G the maximum updrafts varied from 5.1 cm s^{-1} (one polynya) to 3.2 cm s^{-1} (10 polynyas).

5.2.5. A single ice edge. The flow properties in the experiments with a single ice edge were basically similar to those shown in Figures 3 to 5, with the exception that the features over the downstream edges were, of course, lacking. For example, there was neither heat nor momentum recapture by the ice, and in the case of an off-ice wind, the maximum vertical velocity was only 2.9 cm s^{-1}, while it was 5.1 cm s^{-1} over the downwind edge of a polynya. It was interesting that a single ice edge caused rising motion over the downwind side both with on-ice and off-ice winds. In the former the small vertical velocities (maximum 1.0 cm s^{-1}) were the result of the increase in roughness (compare to *Andreas et al.* [1984]), while in the latter it was the surface heat that produced the convection.

5.2.6. Cloudiness. Generally, open water induced rising motions resulting in cloud formation (relative humidity reaching 100%), but clouds were also sometimes formed upwind of polynyas (the initial relative humidity was 90% with no clouds). In the case of no open water the whole model domain was covered by fog from 2 to 600 m, while in the case of no ice a continuous cloud cover was formed at 1 km (a cloud is lifted fog in the model). With a single polynya and G perpendicular to it, a typical situation was of fog forming over the polynya and extending up to 350 m. Over the polynya and downwind of it a cloud cover existed between 200 and 600 m. With parallel G the polynya was typically covered by cloud at 1-2 km, but usually, there was no fog in the model domain. With an ice patch surrounded by open ocean a thin cloud at 1 km overcast the domain. The experiments with several polynyas resulted in basically similar cloudiness to that of a single polynya, except that the cloud cover became more uniform when the number of polynyas increased.

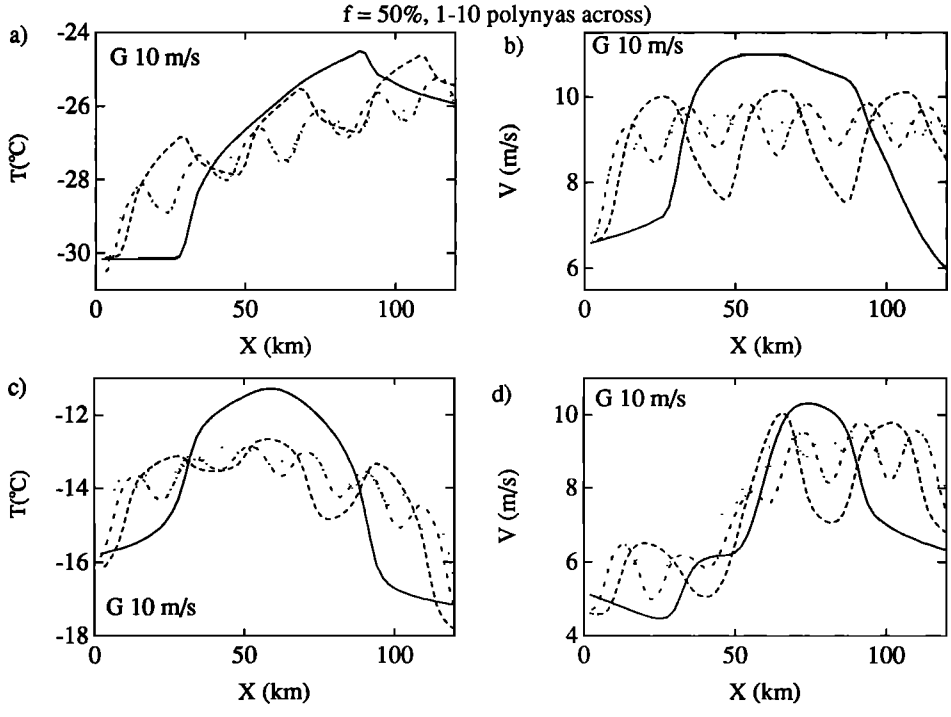

Figure 6. Air temperature and wind speed at a height of 10 m across the model domain with the following numbers of polynyas: one (solid line), three (dashed line), six (dot-dashed line), and 10 (dotted line). (a) Air temperature with G perpendicular to the polynyas. (b) Wind speed with G perpendicular. (c) Air temperature with G parallel. (d) Wind speed with G parallel.

5.2.7. Blending height. A blending height b has been suggested for surface flux calculations using equations (1c) and (2a). In our simulations the blending height was, however, not very well defined. The flow only approached horizontal homogeneity at heights at which it was already far from local equilibrium. This was probably because the extreme differences in the surface temperature considerably modified the flow field. Yet it was usually possible to find z_{min}, a height at which the sum of deviations from local equilibrium and deviations from horizontal homogeneity attained a minimum. *Claussen* [1990] derived the following equation: $z_{min} = 0.7z_0(L_c/z_0)^{4/5}$. According to *Mason* [1988], b should depend on the flow and terrain as $b = 2[u_*/V(b)]^2L_c$, where L_c is the horizontal length scale of each region of different z_0. In the present study, however, a strong dependence of z_{min} on the surface layer stability was found. In the cases with a polynya surrounded by sea ice (unstable) the average z_{min} was 63 m, while in the cases of an ice patch surrounded by open ocean (stable) it was 11 m. Claussen's equation, which is not sensitive to stability, yielded results differing substantially from the present model results. The discrepancy probably resulted from horizontal scales different from those in our study. The estimates based on Mason's equation were of the right order of magnitude but were too high in strongly stable cases and too sensitive to L_c. In the following we shall parameterize the fluxes using various reference heights and compare the results.

5.3. Grid-Averaged Surface Fluxes

The area-averaged surface fluxes of sensible and latent heat as a function of ice coverage in the single-polynya cases are presented in Figure 7. The marked difference between the cases of a polynya surrounded by sea ice and a sea ice patch surrounded by open ocean is very evident. (Remember that the initial θ_{2m} at the inflow boundary was set equal to the local θ_S. Therefore cases with $f = 1$ and $f = 0$ are not drawn in Figure 7 when the upstream θ_Z changes.) In general, $\langle H \rangle$ and $\langle \lambda E \rangle$ increase almost linearly with f. Here $\langle \lambda E \rangle$ was positive (i.e., evaporation) in all cases studied and $\langle Q_L \rangle$ was usually positive (upward) and larger in cases with less clouds (parallel G). With perpendicular G, $\langle \tau \rangle$ increases with f, as did $\langle H \rangle$ and $\langle \lambda E \rangle$, but no clear trend can be detected with parallel G.

Figure 8 shows that $\langle H \rangle$, $\langle \lambda E \rangle$, and $\langle Q_L \rangle$ do not depend much on the spatial scale of the surface variations, as long as the fraction of open water remains the same. The lack of major dependence suggests that the heat and moisture exchange is determined by the local near-surface conditions. The $\langle \tau \rangle$, however, increases with the increasing frequency of surface variations. The variations in surface roughness act as an additional roughness of a larger scale [*Vihma and Savijärvi,* 1991], and it seems that the variations in stability have a similar effect on $\langle \tau \rangle$ ($\langle V \rangle$ was not sensitive to the number of polynyas).

5.4. Vertical Distribution of Heat

Explicit modeling for the rise of a heat plume from a polynya affected by entrainment processes would require a large-eddy resolving model. In the present model the growth of the internal boundary layer was due to turbulent diffusion (described by the mixing length theory) and mesoscale circulations. In addition, processes such as roll circulations on a scale of about 1 km could enhance the entrainment [*Brümmer et al.,* 1994]. Accordingly, the model results merely represent a lower limit for the plume rise. A better study of the topic would also require simulations with a larger variety of initial conditions such as surface temperature, background stability, and wind speed. Despite these reservations we briefly present the model results.

G perpendicular to a polynya resulted in the highest plume rise, usually ($f > 0.1$) extending up to 600 m (700 m when the 50-level model was used; see section 6.2), where the air temperature above and downwind of the polynya still exceeded the upstream value by 1-2°C. Equation (13) derived for narrower leads by *Glendening and Burk* [1992] generally predicts a higher plume rise than obtained by the mesoscale model, for example, 2800 m for the case with $f = 0.5$ (single polynya). The plume rise was only slightly reduced with an increasing number (decreasing width) of polynyas n, e.g., with $n = 10$ the warming at the height of 600 m was some 80% of that with $n = 1$.

With parallel G, warming of at least 1°C reached a height of 350 m (500 m with the 50-level model) with $f = 0.1$-0.5. When an ice patch was surrounded by open ocean, the cooling effect was smaller; even a fetch of 108 km over the ice resulted in a cooling of no more than 1°C at a height of 100 m. In general, the heights affected by the surface heating were well above the typical lowest level of a GCM.

5.5. Further Experiments

The primary simulations were made to study the effects of open ocean fraction, width and number of polynyas, direction of the geostrophic wind with respect to the polynya, and the distribution of surface layer stability (polynya or ice in the middle of the model domain). In addition, there are several other topics which are of interest, and thus we made some more simulations.

5.5.1. Geostrophic wind speed. The first topic chosen is the importance of the geostrophic wind speed. The standard case with $f = 0.5$ and G perpendicular to a polynya (group 1) was also simulated with $G = 3$, 5, 7, 15, and 20 m s^{-1}. The flow properties were basically similar to the run with $G = 10$ m s^{-1}, but naturally the turbulent fluxes were proportional to G, $\langle H \rangle$ ranging from 80 W m^{-2} ($G = 3$ m s^{-1}) to 530 W m^{-2} (20 m s^{-1}). However, with small G the modification in air temperature over the polynya was more effective, because the crossing of the polynya took more time. With $G = 3$ m s^{-1}, θ_{10m} increased by 8.1°C over the polynya, while the increase was only 4.6°C with $G = 20$ m s^{-1}. The wind speed adjusted faster to changed surface conditions when G was smaller. Thus, with $G = 3$ m s^{-1} the maximum near-surface wind speed was reached near the upwind edge of the polynya but only near the downwind edge with $G = 20$ m s^{-1}. The fields of air temperature and wind speed were reflected in the surface fluxes; with $G = 3$ m s^{-1}, H decreased with fetch over the polynya, but with $G = 20$ m s^{-1}, H slightly increased with fetch.

5.5.2. Surface wind acceleration. A strong increase in wind speed over the polynya was observed in all of the simulations, even up to 100% in the case of a single 60-km-wide polynya. The increase may result both from the reduced roughness and the change in stability. A control run with smooth ice replacing the polynya ($z_0^i = 5 \times 10^{-5}$m, i.e., the same as for water) showed a less than 10% wind speed

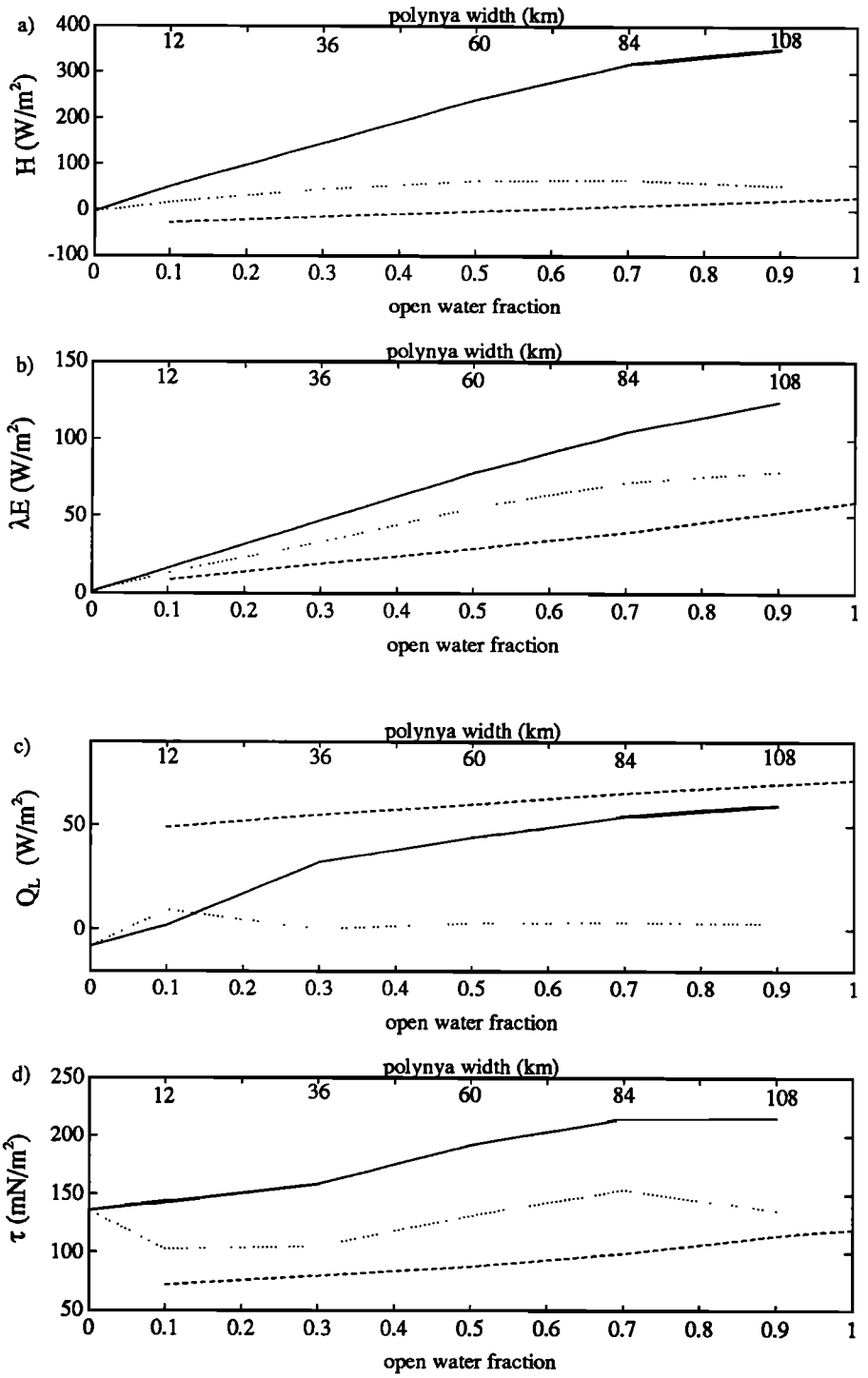

Figure 7. Grid-averaged surface fluxes as a function of the open water fraction. (a) Sensible heat flux. (b) Latent heat flux. (c) Net longwave radiation. (d) Momentum flux. The solid lines denote cases with G perpendicular to a polynya surrounded by ice, the dotted lines denote cases with G parallel to a polynya, and the dashed lines denote cases with G perpendicular to an ice patch surrounded by open ocean.

increase, suggesting that the change in stability was far more important than the reduced roughness. In all of the simulations the momentum flux was also larger over the polynya than over the ice.

5.5.3. Countergradient fluxes. None of the model runs presented so far resulted in countergradient fluxes. A simulation with a thicker snow cover (0.4 m) and a lower polynya fraction (3%) was made to produce these. The results were $\langle H \rangle$ = 2 W m^{-2}, $\langle \theta_s \rangle$ = -36.5°C, and $\langle \theta_{2m} \rangle$ = -36.4°C. Although the mixture methods could not reproduce the right direction of $\langle H \rangle$, the error would be negligible in the cases studied. The countergradient effect may, however, be very important when narrow leads are considered [*Stössel and Claussen*, 1993; *Grötzner et al.*, 1994].

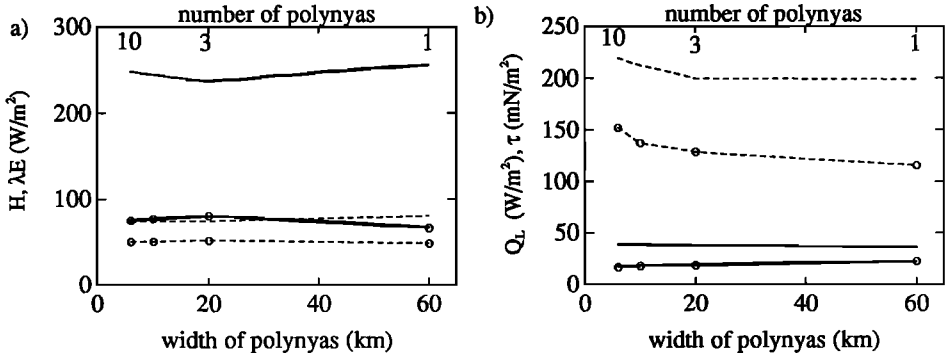

Figure 8. Grid-averaged surface fluxes as a function of the polynya width and the number of polynyas. The lines with (without) circles represent simulations with the geostrophic wind parallel (perpendicular) to the ice edge showing (a) sensible (solid lines) and latent (dashed lines) heat flux and (b) net longwave radiation (solid lines) and momentum flux (dashed lines).

6. Applicability of the Parameterization Schemes

6.1. Turbulent Heat Fluxes

The steady state model results were analyzed, and the air temperature, wind speed, and surface temperature over water and over ice were averaged over the whole model domain to represent the quantities known for the hypothetical GCM. The grid-averaged flux of sensible and latent heat was parameterized using the following four different equations: (1b), (1c), (2a), and (4). Using (1c), Z_t^{eff} was calculated as a logarithmic area average of the local z_t^i and z_t^w, and u_*^2 and L_m^{eff} were calculated from the grid-averaged quantities. When applying (4), $V^{i,w}$ and $\theta^{i,w}$ were first calculated according to (3) using the following weighting factors: g_V = 0.5 and g_θ = 0.2. The values were estimated on the basis of the flow properties and are discussed in section 6.2. The parameterized results compared to those from the 2-D model are presented in Figure 9. The mean absolute deviation from the 2-D model result

$$\frac{}{|\langle H(\text{model})\rangle - \langle H(\text{parameterized})\rangle|}$$

for each parameterization scheme is given in Tables 2 and 3. Because the case with some 10% open water fraction with a polynya in the middle of the ice field represents a typical situation in polar oceans, results for this case are given separately. The mesoscale model levels close to z_{min} in various flow situations were used as reference heights in the calculations and are given in Tables 2 and 3.

We see from the results that the parameterized $\langle H\rangle$ is almost always too small. We can seek the reason from the flow properties (Figures 3 to 6). The subgrid variations in air temperature affect the parameterized $\langle H\rangle$ in the following way: over the ice, $\langle\theta_Z\rangle$ is higher than the true local θ_Z^i, resulting in too small a flux (too large downward), while over the open water, $\langle\theta_Z\rangle$ is lower than the true local θ_Z^w, resulting in too large a flux. The effects compensate each other, but subgrid variations in the wind speed have a monotonic effect; over the ice, $\langle V_Z\rangle$ is too high, resulting in too small a flux (too large downward), while over the open water, $\langle V_Z\rangle$ is too low, again reducing the flux. Thus the parameterized $\langle H\rangle$ remains too small, if the effect is not accounted for. For this reason, (4) gives somewhat better results than the other schemes. The effect is the same both for the mixture and the mosaic method, both for a polynya surrounded by ice and an ice patch surrounded by open ocean, and both for perpendicular and parallel G. For the latent heat flux the effect was not the same, because the flux was upward over the ice as well. This would also be the case for $\langle H\rangle$ over a thin ice cover.

The accuracy of the parameterization methods is typically of the order of 10-20 W m^{-2} in simulations with a polynya surrounded by ice and about 5-10 W m^{-2} in cases with smaller $\langle H\rangle$ with G perpendicular over an ice patch. Particularly large errors occur with the flow over a very large polynya (f = 0.9 in Figure 9a) and with an off-ice flow over a single ice edge. In the latter case, $\langle H\rangle$ was 220 W m^{-2}, but (1b) produced only 134 W m^{-2}.

6.2. Sensitivity Tests

6.2.1. Vertical resolution of the mesoscale model. The principal simulations were made using a 10-level version of the mesoscale model, with a high resolution near the ground and a lower one in the upper layers. This was supposed to be adequate, because the surface fluxes are determined by the differences between the ground and the reference level of 10-100 m. The simulation of processes higher up might, however, suffer from the lower vertical resolution (although the 10-level model was well validated by *Savijärvi* [1991] both in convective and stable conditions). These processes may have indirect influence in the surface layer as well. A 50-level version of the model was therefore built extending the vertical grid up to 6 km, and a couple of control runs were made. The cases with 50% polynya fraction both with perpendicular and parallel wind were selected. The results demonstrated that the flow properties and the surface fluxes were very close to those produced by the 10-level model. The vertical velocities were, however, reduced, and this slightly affected the formation of clouds. This yielded local differences in the surface longwave radiation but not much in the rest of the surface fluxes (in sensible heat flux the results were the same within 3-4 W m^{-2}). The applicability of the parameterization schemes was not affected; the best results were again produced by (4). Thus we regard the results obtained with the 10-level model as reasonably reliable.

6.2.2. Wind speed. When G ranged from 3 to 20 m s^{-1}, the applicability of the parameterization schemes of (1a) - (4)

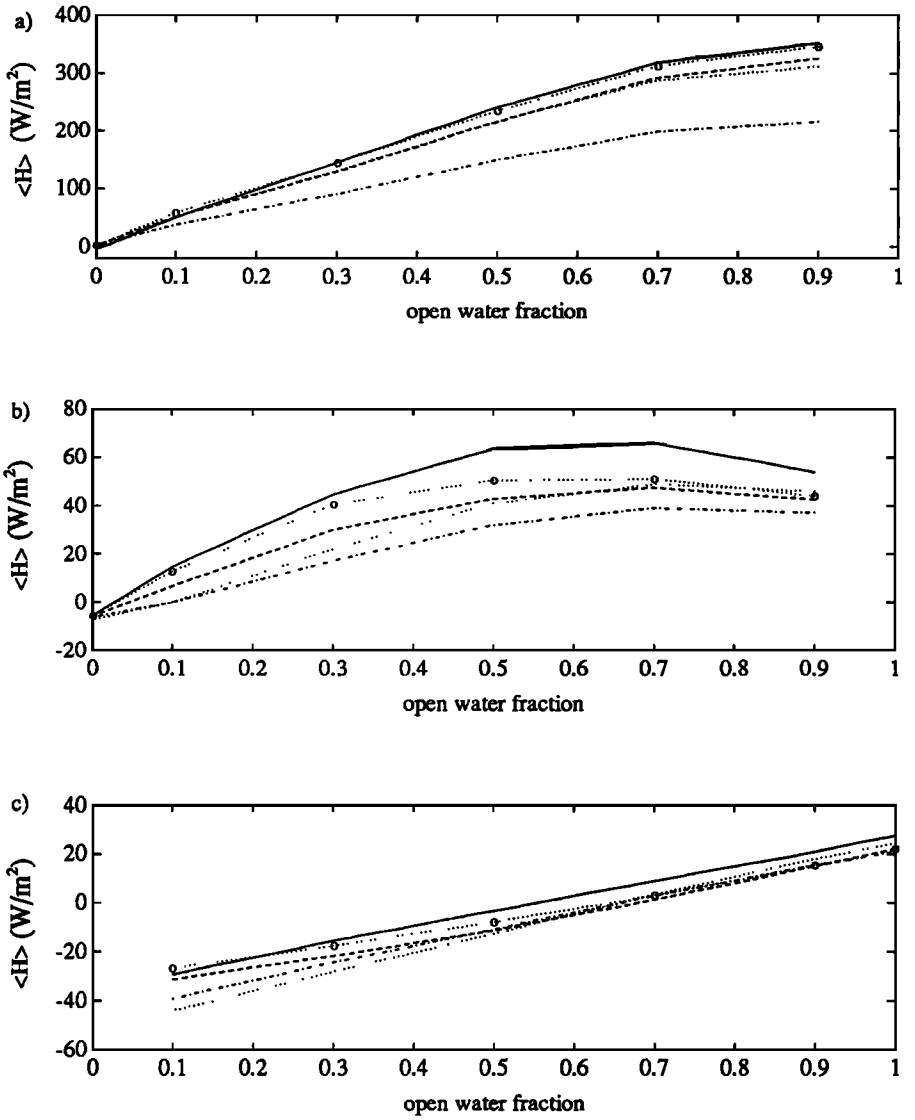

Figure 9. Applicability of the following various schemes to parameterize <*H*>: the mesoscale model result (solid lines) and parameterized results using equations (1b) (dot-dashed lines), (1c) (dotted lines), (2a) (dashed lines), and (4) (dotted lines with circles) for a polynya surrounded by sea ice and (a) perpendicular *G* and (b) parallel *G*, and (c) an ice patch surrounded by open ocean.

Table 2. Mean Absolute Error in Grid-Averaged Turbulent Sensible Heat Flux <*H*>.

	One Polynya, varying width and f				f = 50%, Number of Polynyas Varies		Single Ice Edge, f = 50%		
Equation	Unstable Cases		Stable	*G*	Unstable	*G*	On-Ice	Off-Ice	Parallel
	All	f = 10%	Cases	Parallel	Cases	Parallel	Flow	Flow	Flow
(1b)	83	13	8	24	74	20	9	86	29
(1c)	22	2	9	17	12	9	6	21	17
(2a)	19	1	6	15	12	13	10	20	13
(4)	5	8	4	9	10	6	7	1	7

All values are in watts per square meter. Here f is open water fraction and *G* is geostrophic wind speed. Reference heights used in calculations are as follows: 100 m in unstable cases, 10 m in stable cases, and 30 m when *G* is parallel to ice edges.

Table 3. Mean Absolute Error in Grid-Averaged Turbulent Latent Heat Flux $\langle \lambda E \rangle$.

Equation	One Polynya, varying width and f				f = 50%, Number of Polynyas Varies		Single Ice Edge, f = 50%		
	Unstable Cases		Stable	G	Unstable	G	On-Ice	Off-Ice	Parallel
	All	f = 10%	Cases	Parallel	Cases	Parallel	Flow	Flow	Flow
(1b)	23	4	1	4	20	4	1	20	5
(1c)	4	1	5	7	9	15	1	4	7
(2a)	1	0	1	1	3	1	4	2	1
(4)	5	2	1	1	8	2	3	8	1

See Table 2 footnotes.

was similar to that in the cases with G = 10 m s^{-1}. Equation (4) produced the best results, and (1b), the worst ones.

6.2.3. Roughness lengths. The sensitivity of some of the methods to different choices of roughness lengths and to functions describing the stability effects was tested. Using the method (1c) the effective roughness length for temperature Z_t^{eff} was basically calculated as a logarithmic area average of the local z_t. According to *Wood and Mason* [1991], Z_t^{eff} should be less than that, but this is not supported by our results. For comparisons we also used the following methods. Z_0^{eff} was first calculated by the method of *Taylor* [1987], and Z_t^{eff} was then obtained from the roughness Reynolds number and Z_0^{eff} applying the formula of *Andreas* [1987] originally developed for local roughness lengths over snow and sea ice. Z_t^{eff} was now below the logarithmic area average, but the fluxes were far too low. We also made calculations with the formula of *Garratt* [1978] developed for rough land surfaces; Z_0^{eff}/Z_t^{eff} = 7. The results were about the same as those obtained using the logarithmic area average for Z_t^{eff}.

6.2.4. Stability effects. The comparison of different methods to parameterize the local stability effects is reasonable, because the iterative procedure used in the mesoscale model [*Launiainen and Vihma,* 1990] is impractical for use in a GCM. It was used in the mesoscale model to get as reliable surface fluxes as possible. In the parameterization schemes (2a) and (4) the iteration procedure was replaced by estimating $10/L$ from the bulk Richardson number Ri_B according to *Donelan* [1982]: $10/L = 6.0 \times Ri_B$ for the stable region and $10/L = 7.6 \times Ri_B$ for the unstable region. This produced a small error of 10 W m^{-2} in the local sensible heat flux over a polynya. Over the stably stratified sea ice the error was close to zero. Other alternatives were to use the analogous forms of *Large and Pond* [1982], *Andreas and Murphy* [1986], or *Launiainen* [1995]. The results did not differ much from those obtained using the form of *Donelan* [1982], the results using *Launiainen* [1995] being closest to the iterative solution. The differences in $H^{i,w}$ arising from the use of various values for the turbulent Prandtl number Pr and von Karman constant k are, however, much larger. Using the ψ functions of *Businger et al.* [1971] with Pr = 0.74 and k = 0.35, the sensible heat flux over a winter polynya was some 50-150 W m^{-2} higher than that based on the ψ functions of *Högström* [1988], with Pr = 1.0 and k = 0.4. We used the latter combination in the mesoscale model and in all of the parameterization schemes where ψ functions are involved.

6.2.5. Subgrid variations in surface roughness. In cases with open sea surrounded or bounded by a rough land surface the grid-averaged heat fluxes are more sensitive to variations in the surface roughness. To study this, we changed the z_0 of ice (1 mm) to a value typical for a land surface (0.3 m) and simulated a flow from land to sea (analogous to the group 6 c case). The results demonstrated a very sensitive dependence of $\langle H \rangle$ on the reference height of the calculations. Reasonable results were obtained using z = 100 m. The modeled result for $\langle H \rangle$ was 220 W m^{-2}, while results of 190, 190 and 230 W m^{-2} were produced by (1c), (2a), and (4), respectively. The errors were extreme, if too low a reference height was used with the mosaic method (2a): with z = 2 m, $\langle H \rangle$ = -140 W m^{-2}, and with z = 10 m $\langle H \rangle$ = 60 W m^{-2}. The problem was that the downward heat flux over the land surface became too large; the local C_H was large, and thus the subgrid variations in the wind speed and air temperature had a strong effect on the local heat flux (over the sea ice the effect remained smaller because of a smaller local z_0). Raising the reference height reduced the subgrid heterogeneity and yielded better results. The errors in $\langle \lambda E \rangle$ were smaller, even with low reference heights, because in the cases studied the flux was always upward. The mixture methods were naturally not as sensitive to the reference height; the simple scheme (1b) produced far too large an $\langle H \rangle$ (with every reference height used), but (1c) of *Wood and Mason* [1991] succeeded far better, producing results ranging from 160 to 190 W m^{-2} with reference heights from 2 to 100 m.

6.2.6. Coefficients in (3). In (3), $\theta_z^{i,w}$ and $V_z^{i,w}$ are calculated as a mixture of the values representing a local equilibrium and a grid average. The method is in accordance with the concept of a blending height. A simple nonweighted average (i.e., $g_V = g_\theta$ = 0.5) produced results close to those presented in Tables 2 and 3 and Figure 9 (generally within 10 W m^{-2}), but values of g_V = 0.5 and g_θ = 0.2 were found to be optimal, if z_{min} (blending height) is used as a reference level. It should be noted that (3) and (4) can produce fairly accurate results for any reference level (in the lowest hundreds of meters), if values of g_V and g_θ optimal for the level are used. Thus, if a GCM has such a vertical resolution that a blending height cannot be applied, reasonable fluxes could still be obtained.

6.3. Net Longwave Radiation

The accuracy of the parameterization of the net longwave radiation depends above all on the distribution of cloudiness. Q_L was calculated using the mixture (6) and mosaic methods (7), as well as an extended mosaic method, in which the cloudiness was also separated into N^i and N^w. Because the flow properties indicated that clouds typically form over the

Table 4. Mean Absolute Error in Grid-Averaged Longwave Radiation Flux $\langle Q_L \rangle$.

Equation	One Polynya, varying width and f				f = 50%, Number of Polynyas Varies		Single Ice Edge, f = 50%		
	Unstable Cases		Stable	G	Unstable	G	On-Ice	Off-Ice	Parallel
	All	f = 10%	Cases	Parallel	Cases	Parallel	Flow	Flow	Flow
(6)	9	1	3	4	1	15	1	16	15
(7)	12	1	2	4	4	16	1	20	16
(7),$N^{i,w}$	8	1	2	4	4	11	1	3	12

See Table 2 footnotes. Reference height for air temperature is 30 m.

polynyas, as large a portion of $\langle N \rangle$ as possible was distributed over the open water; $N^w = \min(1, \langle N \rangle / f)$ and $N^i = (\langle N \rangle - fN^w)/(1-f)$.

Considering the results in general, the difference between the mixture and the mosaic approaches with respect to the surface temperature was small, and the reference height for air temperature in (6) and (7) had only a minor effect. The results are shown in Figure 10 (selected cases) and Table 4 (all cases). The absolute errors were usually small, mostly less than 10 W m^{-2} and never exceeding 20 W m^{-2}. The relative error was, however, large in certain cases (perpendicular G across a polynya, parallel G with several polynyas, single ice edge). These cases involved subgrid variations in cloudiness; both the mixture and mosaic methods succeeded well only if the cloud cover was uniform, as with f = 0 and 0.1 in Figure 10a. If the variations were systematic (clouds over open water, clear skies over ice), the mosaic method with separated cloudiness $N^{i,w}$ considerably improved the results. An example is given in Figure 10b: an off-ice wind results in completely clear skies over the ice and continuous cloudiness over the open ocean, and methods using $\langle N \rangle$ fail.

6.4. Momentum Flux

The principal groups of simulations (1-6, compare Table 1a) were analyzed to parameterize $\langle \tau \rangle$, the portion of the grid-averaged momentum flux arising from skin friction, using (8) - (12). Additionally, the results of the sensitivity tests with G varying from 3 to 20 m s^{-1} were used. In general, the performance of the parameterization schemes, based on surface wind, varied from case to case, (8) being, on the average, closest to the model results. When G was varied and f was constant, the choice of reference height for the calculations did not affect the results much, but when f was varied the lowest reference heights (2 and 10 m) produced the best results. Thus the stability effect was best described using a low reference height. The method of calculating separate surface wind speeds over the ice and over the open water was tested, but now it did not improve the results. The performance of (8) - (12) is shown in Figure 11 and Table 5.

Equation (12) was used to parameterize $\langle \tau \rangle$ on the basis of the surface pressure field. First, the geostrophic drag coefficient C_G was estimated on the basis of the model results. There are several variables, e.g., $10/L$ and the Richardson number, which could describe the dependence of C_G on stratification. These were tested, but it was found best to calculate C_G simply from $\langle \theta_S \rangle - \langle \theta_Z \rangle$. The reference height for θ_Z can be anything from 10 m to 1 km, the lower reference heights (e.g., 30 m) producing somewhat better results. A linear relationship was found from the model results in different flow situations:

$$C_G = 0.00075(\langle \theta_S \rangle - \langle \theta_{30m} \rangle) + 0.0286 \qquad (14)$$

The constants would vary slightly for reference heights other than 30 m. In practice, the lowest level of a GCM would be a good choice for the reference height. The results shown in Figure 11 and Table 5 were obtained using (14) with (12). We see that (12) gives practically as good results as the methods based on the surface wind, (8) - (11). The uncertainty is, in general, of the order of 10-30 mN m^{-2}. Moreover, the

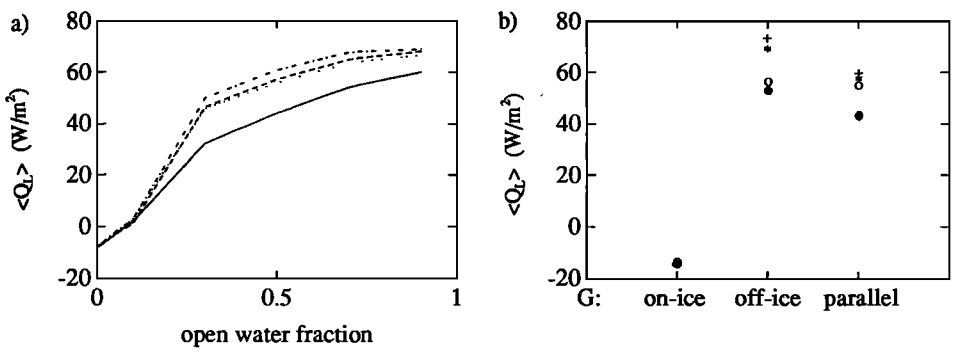

Figure 10. Applicability of the following various schemes to parameterize $\langle Q_L \rangle$: (a) perpendicular G over a polynya surrounded by sea ice and (b) a single ice edge with three flow situations. The mesoscale model result (solid line, solid circles) and parameterized results using equations (6) (dashed line, stars) and (7) (dot-dashed line, crosses), and (7) with cloudiness also separated (dotted line, open circles).

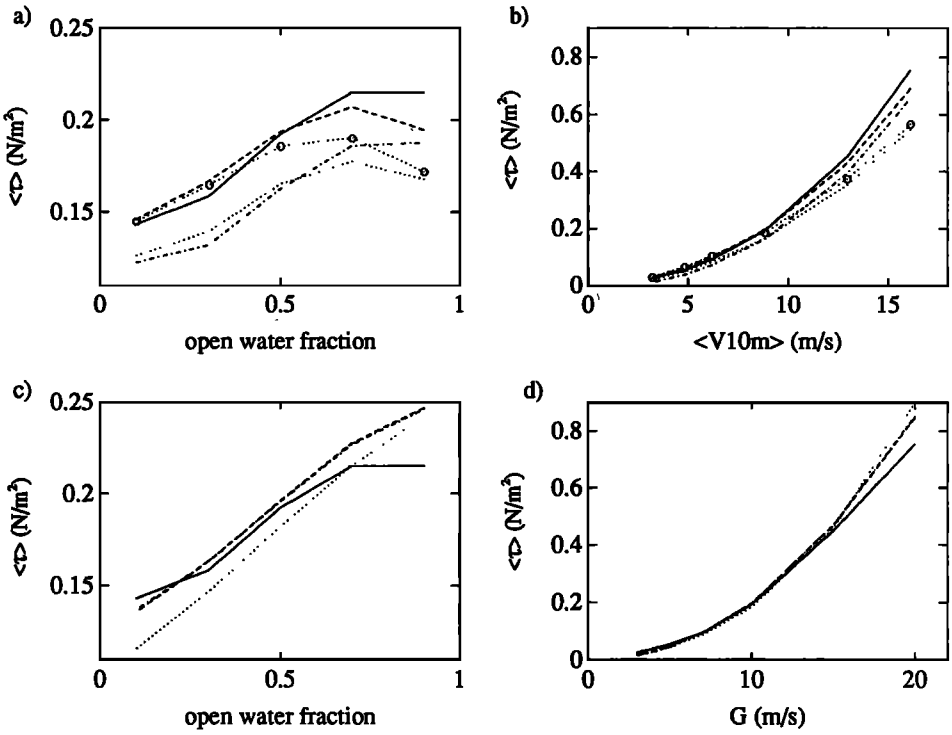

Figure 11. Grid-average of surface momentum flux as a function of the open water fraction (a,c) and wind speed (b,d). The mesoscale model results (solid lines) and parameterized results based on the surface wind are drawn in (a) and (b); parameterized results using equation (8), (dashed lines), (9) (dot-dashed lines), (10) (dotted lines), and (11) (dotted lines with circles). The mesoscale model results (solid lines) and parameterized results based on (12) with C_G from (14) are drawn in (c) and (d); reference heights 30 m (dashed lines), 100 m (dot-dashed lines) and 1 km (dotted lines).

surface winds over polar oceans are uncertain in any models. They depend interactively on the surface momentum flux but also on the momentum exchange at upper levels of the atmospheric boundary layer. Therefore we feel that the most reasonable way to parameterize surface momentum flux is the use of C_G. Knowledge of its dependence on stability is, however, vital to get accurate results.

7. Discussion

The parameterization of surface heat and momentum fluxes over ice-covered oceans was studied considering cases with large areas of open water. The following wide group of cases was studied: a single polynya of varying width in the middle of an ice field, an ice patch of varying width surrounded by open ocean, varying number of polynyas in the ice field, and a single ice edge. The simulations were made using different directions of the geostrophic wind. In addition to the turbulent surface heat fluxes, we examined the surface momentum flux and the net longwave radiation flux at the surface. The vertical distribution of heating was studied as well.

The basic problem for the study was how to produce a grid-averaged surface heat flux using the following variables

Table 5. Mean Absolute Error in Grid-Averaged Skin Drag <τ>.

Equation	One Polynya, varying width and f				f = 50%, Number of Polynyas Varies		Single Ice Edge, f = 50%
	Unstable Cases		Stable	G	Unstable	G	Off-Ice Flow
	All	f = 10%	Cases	Parallel	Cases	Parallel	
(8)	8	5	3	11	5	8	18
(9)	27	10	21	26	30	33	39
(10)*	30	7	17	22	30	26	59
(11)	16	7	2	17	15	11	49
(12)†	12	11	7	13	4	11	23

Reference height is 30 m with all the equations.
* Z_0^{eff} from *Taylor*'s [1987] method was used.
† Equation (14) was used for C_G when applying (12).

known in a GCM: $\langle\theta_Z\rangle$, $\langle\theta_S\rangle$, $\langle q\rangle$, and $\langle V\rangle$, in cases with large subgrid variations in these variables. The simplest methods are based on direct parameterization with $\langle\theta_Z\rangle$, $\langle\theta_S\rangle$, $\langle q_Z\rangle$, and $\langle V\rangle$ and an effective transfer coefficient or roughness length for temperature (mixture method). Another alternative is the mosaic method, a separation of the ice-covered and ice-free parts of the grid square, both having a specific surface temperature. Even so, the subgrid variations in air temperature and humidity, wind speed, and (for radiative fluxes) cloudiness pose a problem. The mosaic method is, however, supposed to work if the leads are narrow [*Claussen*, 1991a].

In lieu of observations to test the parameterization schemes, a 2-D mesoscale model was applied to produce fields of θ_Z, θ_S, q_Z, V, H, λE, Q_L, and τ. The flow fields showed large variations in near-surface air temperature, specific humidity, and wind speed. The variations were mostly caused by stability effects which dominated the effects of the roughness difference between the ice and open water. The wind speed reacted rapidly to changed surface conditions. The fluxes varied substantially between different flow situations (cold air advected over a polynya, warm air advected over ice, parallel flow), as seen in Figure 7, but the applicability of the parameterization schemes did not depend much on the flow situation.

Considering the turbulent surface heat fluxes, the results can be summarized as follows. The use of transfer coefficients dependent on stability is essential. Neutral transfer coefficients (1b), which are still used in some models, can yield errors of 70-80 W m^{-2} in $\langle H\rangle$ and 20 W m^{-2} in $\langle\lambda E\rangle$. Equations (1c) and (2a) produced far better results. The success of the mosaic method (2a) was partially based on the fact that although the subgrid variations in the near-surface air temperature could exceed 10°C, the errors in the local heat fluxes due to this effect over the ice and over open water tended to balance each other. However, the effect of subgrid variations in wind speed dominated the air temperature effect, the high wind speeds accompanying upward H. The parameterized $\langle H\rangle$ was therefore typically too small. Any trick yielding higher transfer coefficients would thus improve the results, but we should account for the true reasons for the deviations. Equation (4) was therefore used, extending the mosaic approach to use $\theta_Z^{i,w}$ and $V_Z^{i,w}$. This generally improved the results. Applying (4), we should, however, bear in mind that over polar oceans the surface wind speed is perhaps the most difficult quantity to be accurately determined from a GCM. The wind acceleration above a warmer sea surface due to increase in θ_S has, in any case, been detected in several field experiments [e.g., *Sweet et al.*, 1981; *Mey et al.*, 1990] and modeling studies [*Overland et al.*, 1983; *Huang and Raman*, 1988; *Wai and Stage*, 1989]. Therefore, even though the grid-averaged surface wind of a GCM is erroneous, it would be reasonable to parameterize the subgrid variations in the wind speed using an equation such as (4).

There are always models in which the parameterization is preferred to be kept as simple as possible. In these the mixture method (1c) of *Wood and Mason* [1991] could be considered. It yields results comparable to the mosaic method (2a), and it is not as sensitive to the calculation height as the latter. As (2a), it produces somewhat too low fluxes because of the subgrid variations in wind speed and the nonlinearity in the flux profile relationships. Yet, it cannot reproduce the right direction when the area-averaged flux is countergradient. This may be serious [*Stössel and Claussen*, 1993; *Grötzner et al.*, 1994], although not in the cases analyzed in this study. In contrast with applications to general conditions [*Wood and Mason*, 1991], we found the logarithmic area average of z_t to be a reasonable approximation for Z_t^{eff} over oceans with winter polynyas. This approximately equals the relation $Z_0^{eff}/Z_t^{eff} \sim 7$, which *Garratt* [1978] found for rough land surfaces with large turbulent fluxes. This kind of estimate could be used for Z_t^{eff}, as long as a validated theory for calculating it is lacking.

The parameterization of local stability effects affects the results. Several practical schemes were compared against an iterative solution of the flux profile relationships of the Monin-Obukhov theory with functions depending on $10/L$ [*Högström*, 1988; *Holtslag and de Bruin*, 1988]. As a result, we found it reasonable to estimate $10/L$ on the basis of the bulk Richardson number.

We also found it applicable for mesoscale situations to use the methods of *Mason* [1988] and *Claussen* [1990, 1991a, b] to compute the turbulent heat fluxes at a blending height. The blending height was not, however, always well defined, and the equations to predict it were not applicable in cases with wide polynyas. The mosaic method (2a) was sensitive to the calculation height, and the use of too low a height caused extreme errors in $\langle H\rangle$, if applied over a coastal area having large subgrid variations in surface roughness. In most of today's GCMs the grid squares in coastal areas are set to be either wholly sea or land, but they could be presented as polynyas using the fraction of land and sea in each grid square. This would allow a more realistic representation of the coastline.

It should be remembered that we assumed through this paper that the surface temperature is a variable in a GCM. If it is specified, e.g., climatologically, far larger errors are to be expected in the surface fluxes. Even if θ_S is calculated in the GCM, it depends interactively on the surface fluxes, and errors in calculating it cause errors in the fluxes as well. Accordingly, the real accuracy of the fluxes that can be expected in a GCM is not quite as good as the results presented in Figure 9 and Tables 2-4 would indicate. (In parameterizing the heat fluxes, we used the true grid-averages of $\langle\theta_S\rangle$ and $\langle\theta_S^i\rangle$ produced by the mesoscale model.) In addition, errors in θ_S would affect the atmospheric surface layer, causing problems, e.g., with the reference level (compare to *Stössel* [1992]).

On the basis of this study, the subgrid heterogeneity can cause parameterization errors of up to 20 W m^{-2} in the grid-averaged net longwave radiation at the surface. The errors result mostly from subgrid variations in cloudiness. If we know the distribution of cloudiness with respect to the polynyas reliably enough, the errors can be reduced by separating the cloudiness into that over open water and that over ice. The mesoscale model used is far from complete in its skill to simulate cloud formation, but the model results are in reasonable agreement with observations [e.g., *Fairall and Markson*, 1987]; clouds tend to form over the open water, where convection is favored. This principle could be used in calculating N^i and N^w from $\langle N\rangle$. Clouds associated, e.g., with transient cyclones do, of course, not follow this rule. The model was not applied to study the parameterization of shortwave radiation, but we feel that (5) should work, if the

cloudiness and surface albedo over ice and open water can be estimated reliably enough.

The parameterization of the surface momentum flux poses a serious problem. Here we considered only the skin drag portion, and we found that the effect of stability variations dominates over the roughness effect. We first tried to parameterize the skin drag on the basis of the near-surface wind speed and stratification, but it seems more reasonable to use the atmospheric surface pressure field and a C_G depending on the air-surface temperature difference. To get the total surface momentum flux, one could proceed along the lines of *Stössel and Claussen* [1993].

As long as the open water fraction remained the same, the number and width of polynyas did not have a strong effect on the surface fluxes of heat and moisture. The momentum flux was affected, however, an increasing frequency of surface variations resulting in increased $<\tau>$.

The vertical distribution of heat rising from polynyas was analyzed, although the process could not be completely resolved by a mesoscale model. The results differed from those predicted by (13), an equation obtained with the aid of a large-eddy simulation model but on the scale of leads. The coupling of processes with different scales remains a problem, but in general, the results demonstrated a need to include an algorithm in GCMs for the vertical distribution of subgrid-scale surface heating.

Fluxes on the scale of turbulence are not the only process affecting the vertical transport on a subgrid scale. For example, *Kottmeier and Engelbart* [1992] observed mesoscale circulations in the atmospheric boundary layer induced by the surface temperature gradient at an Antarctic ice shelf front. Our mesoscale model also produced such circulations, as described in section 5.2. The circulations transported heat and moisture upward, the flux divergences tending to cool and dry the lowest hundreds of meters and heat and moisten the layers above. Parameterization of these mesoscale fluxes is the topic of a paper in preparation.

8. Conclusions

The basic results of this study could easily be applied in GCMs as follows. (1) Parameterize the turbulent surface heat fluxes using an extended mosaic method with estimates for the air temperature and wind speed over the ice and open water. Use a reference height of the order of 100 m, if the overall stratification is unstable, and of the order of 10 m if stable. Since the GCM does not necessarily provide values at these heights, the values at the GCM grid levels should somehow be interpolated to the blending height. (2) Parameterize the radiative flues at the surface using the mosaic method with estimates for albedo and cloudiness over the ice-covered and ice-free parts of the grid square. (3) Parameterize the skin drag portion of the surface momentum flux on the basis of the atmospheric pressure field using a geostrophic drag coefficient dependent on the air-surface temperature difference.

According to the study of *Chapman et al.* [1994], the lead fraction and the sensible heat and momentum transfer coefficients were the parameters to which an Arctic sea ice model was most sensitive. Thus great benefit would come from efforts to discover optimal methods for calculating the heat and momentum exchange processes. As the mesoscale model results are not complete, these efforts should also include observations of the polar atmospheric boundary layer, not only over narrow leads, but also on the mesoscale.

Acknowledgments. I am grateful to Hannu Savijärvi for providing me with the 2-D mesoscale model. Jouko Launiainen and Hannu Savijärvi are acknowledged for comments on the manuscript and Alexander Makshtas, James E. Overland, and Dirk Dethleff (who also provided me with a satellite image for Figure 1) for discussions. I thank Martin Claussen and two other reviewers for their comments and suggestions.

References

Alestalo, M., and H. Savijärvi, Mesoscale circulations in a hydrostatic model: Coastal convergence and orographic lifting, *Tellus, Ser. A, 37A,* 156-162, 1985.

Andreas, E.L., A theory for the scalar roughness and the scalar transfer coefficients over snow and sea ice, *Boundary Layer Meteorol., 38,* 159-184, 1987.

Andreas, E.L., and A.P. Makshtas, Energy exchange over Antarctic sea ice in the spring, *J. Geophys. Res., 90,* 7199-7212, 1985.

Andreas, E.L., and B. Murphy, Bulk transfer coefficients for heat and momentum over leads and polynyas, *J. Phys. Oceanogr., 16,* 1875-1883, 1986.

Andreas, E.L., C.A. Paulson, R.M. Williams, R.W. Lindsay, and J.A. Businger, The turbulent heat flux from Arctic leads, *Boundary Layer Meteorol., 17,* 57-91, 1979.

Andreas, E.L., W.B. Tucker, and S.F. Ackley, Atmospheric boundary layer modification, drag coefficient, and surface heat flux in the Antarctic marginal ice zone, *J. Geophys. Res., 89,* 649-661, 1984.

Arya, S.P.S., A drag partition theory for determining the large-scale roughness parameter and wind stress on the Arctic pack ice, *J. Geophys. Res., 80,* 3447-3454, 1975.

Bromwich, D.H., and D.D. Kurtz, Katabatic wind forcing of the Terra Nova Bay polynya, *J. Geophys. Res., 89,* 3561-3572, 1984.

Brümmer, B., B. Busack, H. Hoeber, and G. Kruspe, Boundary-layer observations over open water and Arctic sea-ice during on-ice air flow, *Boundary Layer Meteorol., 68,* 75-108, 1994.

Businger, J.A., J.C. Wyngaard, Y. Izumi, and E.F. Bradley, Flux-profile relationships in the atmospheric surface layer, *J. Atmos. Sci., 28,* 181-189, 1971.

Cavalieri, D.J., and S. Martin, A passive microwave study of polynyas along the Antarctic Wilkes Land coast, in *Oceanology of the Antarctic Continental Shelf, Antarct. Res. Ser.,* vol. 43, edited by S.S. Jacobs, pp. 227-252, AGU, Washington, D.C., 1985.

Chapman, W.L., W.J. Welch, K.P. Bowman, J. Sacks, and J.E. Walsh, Arctic sea ice variability: Model sensitivities and a multidecadal simulation, *J. Geophys. Res., 99,* 919-935, 1994.

Claussen, M., Area-averaging of surface fluxes in a neutrally stratified, horizontally inhomogeneous atmospheric boundary layer, *Atmos. Environ. Part A, 24A,* 1349-1360, 1990.

Claussen, M., Local advection processes in the surface layer of the marginal ice zone, *Boundary Layer Meteorol., 54,* 1-27, 1991a.

Claussen, M., Estimation of areally-averaged surface fluxes, *Boundary Layer Meteorol., 54,* 387-410, 1991b.

Comiso, J.C., and A.L. Gordon, Recurring polynyas over the Cosmonaut Sea and the Maud Rise, *J. Geophys. Res., 92,* 2819-2833, 1987.

den Hartog, G., S.D. Smith, R.J. Anderson, D.R. Topham, and R.G. Perkin, An investigation of a polynya in the Canadian archipelago, 3, Surface heat flux, *J. Geophys. Res., 88,* 2911-2916, 1983.

Dethleff, D., Polynyas as a possible source for enigmatic Bennett Island atmospheric plumes, in *The Polar Oceans and Their Role in Shaping the Global Environment, Geophys. Monogr. Ser.,*

vol. 85, edited by O.M. Johannessen, R.D. Muench, and J.E. Overland, pp. 475-483, AGU, Washington, D.C., 1994.

Donelan, M.A., The dependence of the aerodynamic drag coefficient on wave parameters, in *Proceedings of First International Conference on Meteorology and Air-Sea Interaction of the Coastal Zone,* pp. 381-387, Am. Meteorol. Soc, Boston, Mass., 1982.

Fairall, C.W., and R. Markson, Mesoscale variations in surface stress, heat fluxes, and drag coefficient in the marginal ice zone during the 1983 Marginal Ice Zone Experiment, *J. Geophys. Res., 92,* 6921-6932, 1987.

Garratt, J.R., Transfer coefficients for a heterogeneous surface of large aerodynamic roughness, *Q. J. R. Meteorol. Soc., 104,* 491-502, 1978.

Glendening, J.W., and S.D. Burk, Turbulent transport from an Arctic lead: A large-eddy simulation, *Boundary Layer Meteorol., 59,* 315-339, 1992.

Gloersen, P., W.J. Campbell, D.J. Cavalieri, J.C. Comiso, C.L. Parkinson, and H.J. Zwally, *Arctic and Antarctic Sea Ice, 1978-1987: Satellite Passive-Microwave Observations and Analysis, NASA Publ. SP-511,* Washington, D.C., 1992.

Grötzner, A., R. Sausen, and M. Claussen, The impact of sub-grid scale sea-ice inhomogeneities on the performance of the atmospheric general circulation model ECHAM, *Rep. No. 143,* 42 pp., Max-Planck-Institut for Meteorology, Hamburg, Germany, 1994.

Hanssen-Bauer, I., and Y.T. Gjessing, Observations and model calculations of aerodynamic drag on sea ice in the Fram Strait, *Tellus, Ser. A, 40A,* 151-161, 1988.

Högström, U., Non-dimensional wind and temperature profiles in the atmospheric surface layer: A re-evaluation, *Boundary Layer Meteorol., 42,* 55-78, 1988.

Holtslag, A.A.M, and H.A.R. de Bruin, Applied modeling of the nighttime surface energy balance over land, *J. Appl. Meteorol., 37,* 689-704, 1988.

Huang, C.-Y., and S. Raman, A numerical modelling study of the marine boundary layer over the Gulf Stream during cold air advection, *Boundary Layer Meteorol., 45,* 251-290, 1988.

Kottmeier, C., and D. Engelbart, Generation and atmospheric heat exchange of coastal polynyas in the Weddell Sea, *Boundary Layer Meteorol., 60,* 207-234, 1992.

Kottmeier, C., and R. Hartig, Winter observations of the atmosphere over Antarctic sea ice, *J. Geophys. Res., 95,* 16,551-16,560, 1990.

Large, W.G., and S. Pond, Sensible and latent heat flux measurements over the ocean, *J. Phys. Oceanogr., 12,* 464-482, 1982.

Launiainen, J., Parameterization of the water vapour flux over a water surface by the bulk aerodynamic method, *Ann. Geophys.,* 1, 481-492, 1983.

Launiainen, J., Derivation of the relationship between the Obukhov stability parameter and the bulk Richardson number for the flux-profile studies, *Boundary Layer Meteorol.,* in press, 1995.

Launiainen, J., and T. Vihma, Derivation of turbulent surface fluxes - An iterative flux-profile method allowing arbitrary observing heights, *Environ. Software, 5,* 113-124, 1990.

Launiainen, J., and T. Vihma, On the surface heat fluxes in the Weddell Sea, in *The Polar Oceans and Their Role in Shaping the Global Environment, Geophys. Monogr. Ser.,* vol. 85, edited by O.M. Johannessen, R.D. Muench, and J.E. Overland, pp. 399-419, AGU, Washington, D.C., 1994.

Ledley, T.S., A coupled energy balance climate-sea ice model: Impact of sea ice and leads on climate, *J. Geophys. Res., 93,* 15,919-15,932, 1988.

Louis, J.P., A parametric model of vertical eddy fluxes in the atmosphere, *Boundary Layer Meteorol., 17,* 187-202, 1979.

Makshtas, A.P., *The Heat Budget of Arctic Ice in the Winter,* 77 pp., Int. Glaciol. Soc., Cambridge, England, 1991.

Marshall, K., Drag measurements in roughness arrays of varying density and distribution, *Agric. Meteorol., 8,* 269-292, 1971.

Mason, P.J., The formation of areally-averaged roughness lengths, *Q. J. R. Meteorol. Soc., 114,* 399-420, 1988.

Maykut, G.A., Energy exchange over young sea ice in the central Arctic, *J. Geophys. Res., 83,* 3646-3658, 1978.

Maykut, G.A., and P.E. Church, Radiation climate of Barrow, Alaska, 1962-66, *J. Appl. Meteorol., 12,* 620-628, 1973.

Mey, R.D., N.D. Walker, and M.R. Jury, Surface heat fluxes and marine boundary layer modification in the Agulhas Retroflection Region, *J. Geophys. Res., 95,* 15,997-16,015, 1990.

Overland, J.E., and R. Colony, Geostrophic drag coefficients for the central Arctic derived from Soviet drifting station data, *Tellus, Ser. A, 46A,* 75-85, 1994.

Overland, J.E., and K.L. Davidson, Geostrophic drag coefficient over sea ice. *Tellus, Ser. A, 44A,* 54-66, 1992.

Overland, J.E., R.M. Reynolds, and C.H. Pease, A model of the atmospheric boundary layer over the marginal ice zone, *J. Geophys. Res., 88,* 2836-2840, 1983.

Pease, C.H., The size of wind-driven coastal polynyas, *J. Geophys. Res., 92,* 7049-7059, 1987.

Savijärvi, H., The United States Great Plains diurnal ABP variation and the nocturnal low-level jet, *Mon. Weather. Rev., 119,* 833-840, 1991.

Savijärvi, H., and T. Siili, The Martian slope winds and the nocturnal PBL jet, *J. Atmos. Sci., 50,* 77-88, 1993.

Schmitt, K.F., C.A. Friehe, and C.H. Gibson, Structure of marine surface layer turbulence, *J. Atmos. Sci., 36,* 602-618, 1979.

Schnell, R.C., R.G. Barry, M.W. Miles, E.L. Andreas, L.F. Radke, C.A. Brock, M.P. McCormick, and J.L. Moore, Lidar detection of leads in Arctic sea ice, *Nature, 339,* 530-532, 1989.

Serreze, M.C., J.A. Maslanik, M.C. Rehder, R.C. Schnell, J.D. Kahl, and E.L. Andreas, Theoretical heights of buoyant convection above open leads in the winter Arctic pack ice cover, *J. Geophys. Res., 97,* 9411-9422, 1992.

Simmons, I., and W.F. Budd, Sensitivity of the southern hemisphere circulation to leads in the Antarctic pack ice, *Q. J. R. Meteorol. Soc., 117,* 1003-1024, 1991.

Smith, S.D., Wind stress and heat flux over the open ocean in gale force winds, *J. Phys. Oceanogr., 10,* 709-726, 1980.

Smith, S.D., Water vapour flux at the sea surface, *Boundary Layer Meteorol., 47,* 227-293, 1989.

Smith, S.D., R.J. Anderson, G. den Hartog, D.R. Topham, and R.G. Perkin, An investigation of a polynya in the Canadian archipelago, 2, Structure of turbulence and sensible heat flux, *J. Geophys. Res., 88,* 2900-2910, 1983.

Smith, S.D., R.D. Muench, and C.H. Pease, Polynyas and leads: An overview of physical processes and environment, *J. Geophys. Res., 95,* 9461-9479, 1990.

Stössel, A., Sensitivity of the Southern Ocean sea-ice simulations to different atmospheric forcing algorithms, *Tellus, Ser. A, 44A,* 395-413, 1992.

Stössel, A., and M. Claussen, On the momentum forcing of a large-scale sea-ice model, *Clim. Dyn., 9,* 71-80, 1993.

Sweet, W., R. Fett, J. Kerling, and P. LaViolette, Air-sea interaction effects in the lower troposphere across the north wall of the Gulf Stream, *Mon. Weather Rev., 109,* 1042-1052, 1981.

Taylor, P.J., Comments and future analysis on effective roughness lengths for use in numerical three-dimensional modelling, *Boundary Layer Meteorol., 39,* 403-418, 1987.

Vihma, T., Effect of polynyas on the grid-averaged heat fluxes, in *Evening Sessions of the Summer School on Physics of Ice-Covered Seas, Savonlinna, Finland, 6-17 June, 1994, Rep. Ser. Geophys.,* vol. 28, edited by T. Vihma, pp. 29-32, Univ. of Helsinki, Helsinki, 1994.

Vihma, T., and H. Savijärvi, On the effective roughness length for heterogeneous terrain, *Q. J. R. Meteorol. Soc., 117,* 399-407, 1991.

Wai, , M.M.-K., and S.A. Stage, Dynamical analysis of marine atmospheric boundary layer structure near the Gulf Stream oceanic front, *Q. J. R. Meteorol. Soc., 115,* 29-44, 1989.

Wood, N., and P. Mason, The influence of static stability on the effective roughness lengths for momentum and heat transfer, *Q. J. R. Meteorol. Soc., 117,* 1025-1056, 1991.

Worby, A.P., and I. Allison, Ocean-atmosphere energy exchange over thin, variable concentration Antarctic pack ice. *Ann. Glaciol., 15,* 184-190, 1991.

Zwally, H.J., J.C. Comiso, and A.L. Gordon, Antarctic offshore leads and polynyas and oceanographic effects, in *Oceanology of the Antarctic Continental Shelf, Antarct. Res. Ser.,* vol. 43, edited by S.S. Jacobs, pp. 203-226, AGU, Washington, D.C., 1985.

T. Vihma, Department of Geophysics, P.O. Box 4, FIN-00014 University of Helsinki, Finland. (e-mail: timo.vihma@helsinki.fi)

(Received November 29, 1994; revised June 9, 1995; accepted June 14, 1995.)